Supplementary Information

YTHDF2 upregulation and subcellular localization dictate CD8 T cell polyfunctionality in anti-tumor immunity

Authors: Haiyan Zhang[1#], Xiaojing Luo[2,3#], Wei Yang[2,4], Zhiying Wu[2,3], Zhicong Zhao[5,10], Xin Pei[1], Xue Zhang[1], Chonghao Chen[1], Josh Haipeng Lei[1], Qingxia Shi[1], Qi Zhao[2,3], Yanxing Chen[2,3], Wenwei Wu[2,3], Zhaolei Zeng[2,3], Huai-Qiang Ju[2,3], Miaozhen Qiu[2,3], Jun Liu[6], Bin Shen[7], Minshan Chen[2,8], Jianjun Chen[5], Chu-Xia Deng[1,4], Rui-Hua Xu[2,3,9]*, Jiajie Hou[1,4,8]*

Affiliations:

[1]Cancer Center, Faculty of Health Sciences, University of Macau, Macau SAR, China; MOE Frontier Science Center for Precision Oncology, University of Macau, Macau SAR, China

[2]State Key Laboratory of Oncology in South China, Collaborative Innovation Center for Cancer Medicine, Sun Yat-sen University Cancer Center, Guangzhou 510060, China

[3]Research Unit of Precision Diagnosis and Treatment for Gastrointestinal Cancer, Chinese Academy of Medical Sciences, Guangzhou 510060, China

[4]Translational Research Center, Zhuhai UM Science & Technology Research Institute, Zhuhai 519031, China

[5]Department of Systems Biology, The Beckman Research Institute of City of Hope, Duarte, CA91010, USA

[6]Peking-Tsinghua Center for Life Sciences, Peking University, Beijing 100871, China

[7]State Key Laboratory of Reproductive Medicine, Nanjing Medical University, Nanjing 211166, China

[8]Department of Liver Surgery, Sun Yat-sen University Cancer Center, Guangzhou 510060, China

[9]Department of Medical Oncology, Sun Yat-sen University Cancer Center, Guangzhou 510060, China

[10]Department of Liver Surgery, Renji Hospital, School of Medicine, Shanghai Jiao Tong University, Shanghai 200127, China

[#]These authors contributed equally: Haiyan Zhang, Xiaojing Luo

*Correspondence: xurh@sysucc.org.cn (R.-H.X.); jiajiehou@um.edu.mo (J.H.)

This Supplementary Information File contains: Supplementary Figures 1–11

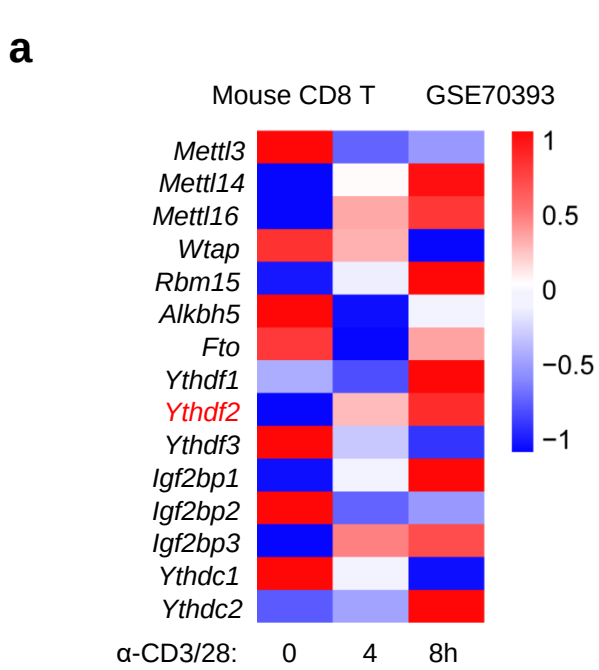
a
Mouse CD8 T
GSE70393
Mettl3
Mettl14
Mettl16
Wtap
Rbm15
Alkbh5
Fto
Ythdf1
Ythdf2
Ythdf3
Igf2bp1
Igf2bp2
Igf2bp3
Ythdc1
Ythdc2
1
0.5
0
−0.5
−1
α-CD3/28: 0 4 8h

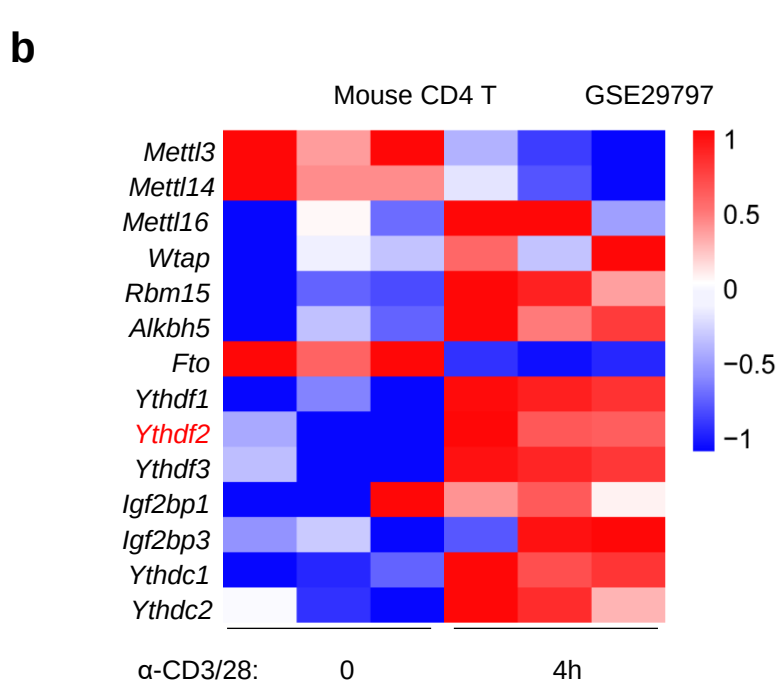
b
Mouse CD4 T
GSE29797
Mettl3
Mettl14
Mettl16
Wtap
Rbm15
Alkbh5
Fto
Ythdf1
Ythdf2
Ythdf3
Igf2bp1
Igf2bp3
Ythdc1
Ythdc2
1
0.5
0
−0.5
−1
α-CD3/28: 0 4h

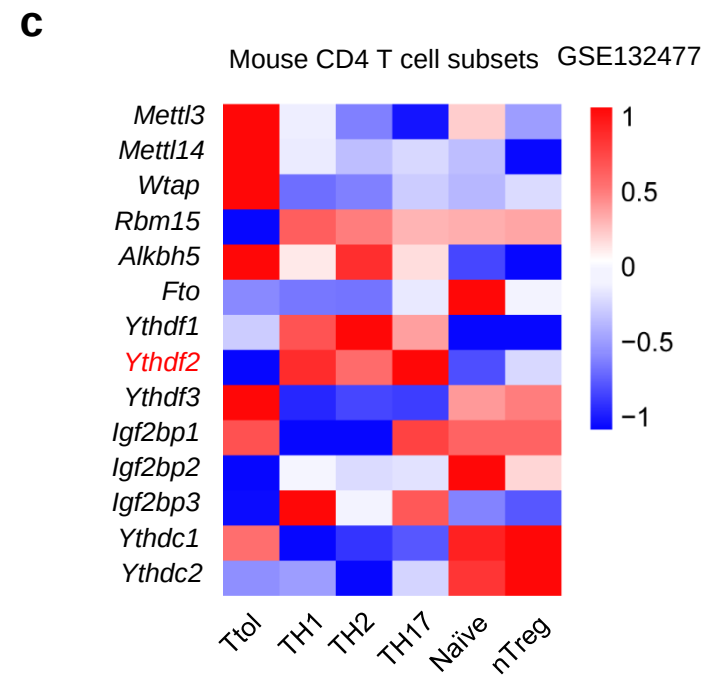
c
Mouse CD4 T cell subsets
GSE132477
Mettl3
Mettl14
Wtap
Rbm15
Alkbh5
Fto
Ythdf1
Ythdf2
Ythdf3
Igf2bp1
Igf2bp2
Igf2bp3
Ythdc1
Ythdc2
1
0.5
0
−0.5
−1
Ttol
TH1
TH2
TH17
Naïve
nTreg

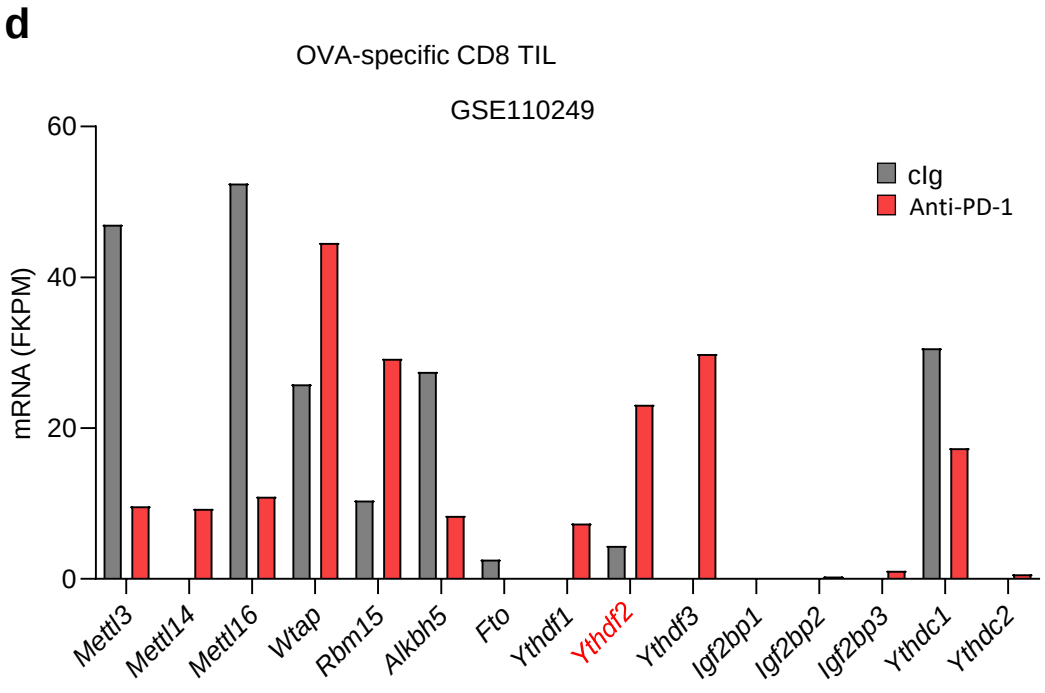
d
OVA-specific CD8 TIL
GSE110249
mRNA (FKPM)
60
40
20
0
cIg
Anti-PD-1
Mettl3
Mettl14
Mettl16
Wtap
Rbm15
Alkbh5
Fto
Ythdf1
Ythdf2
Ythdf3
Igf2bp1
Igf2bp2
Igf2bp3
Ythdc1
Ythdc2

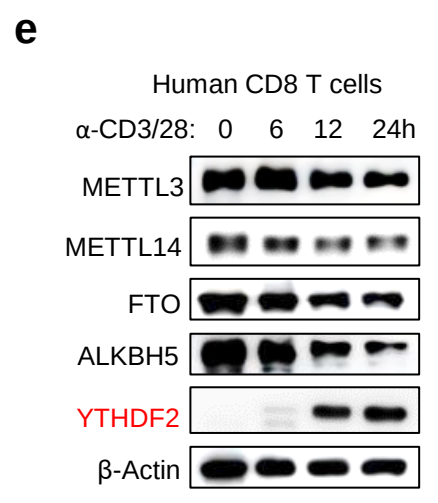
e
Human CD8 T cells
α-CD3/28: 0 6 12 24h
METTL3
METTL14
FTO
ALKBH5
YTHDF2
β-Actin

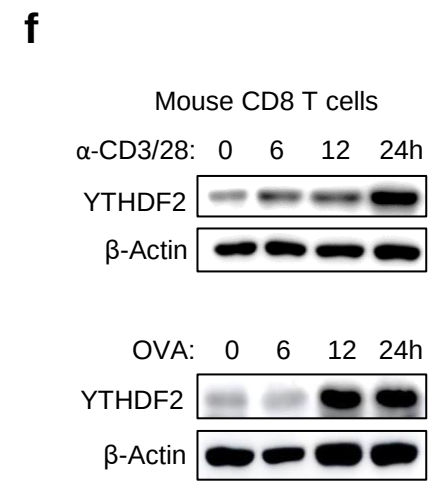
f
Mouse CD8 T cells
α-CD3/28: 0 6 12 24h
YTHDF2
β-Actin
OVA: 0 6 12 24h
YTHDF2
β-Actin

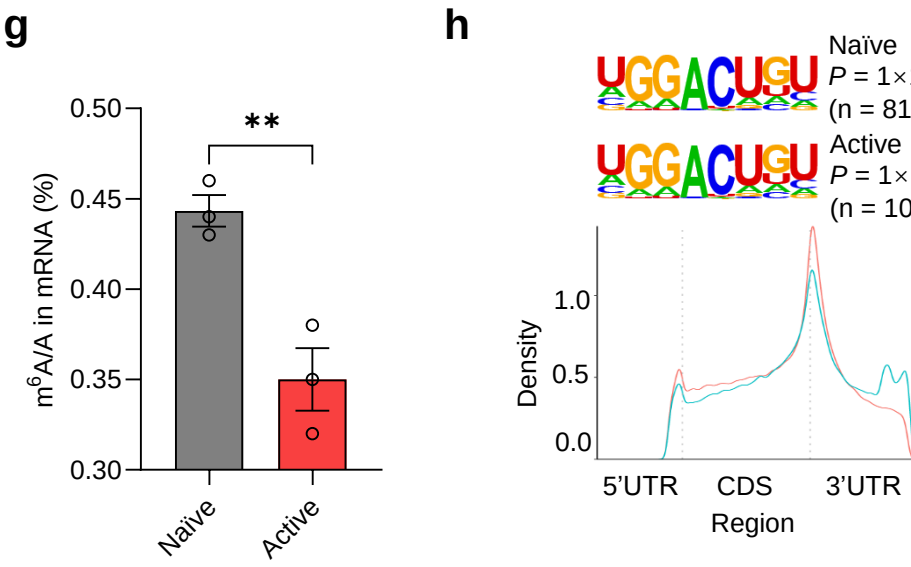
g
m6A/A in mRNA (%)
0.50
0.45
0.40
0.35
0.30
**
Naïve
Active

h
Naïve
P = 1×10-620
(n = 8166)
Active
P = 1×10-870
(n = 10302)
Density
1.0
0.5
0.0
5'UTR
CDS
3'UTR
Region

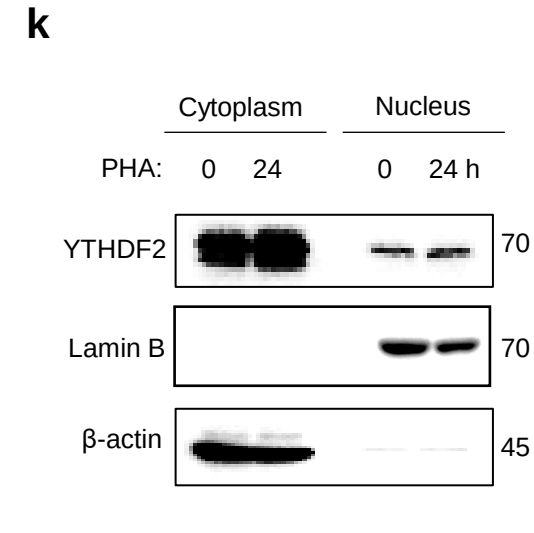
k
Cytoplasm
Nucleus
PHA: 0 24 0 24 h
YTHDF2
70
Lamin B
70
β-actin
45

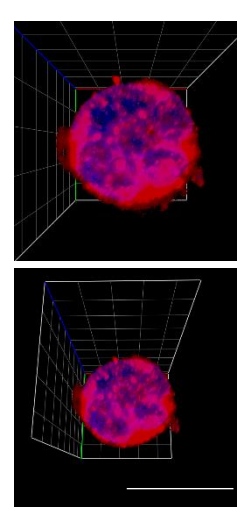

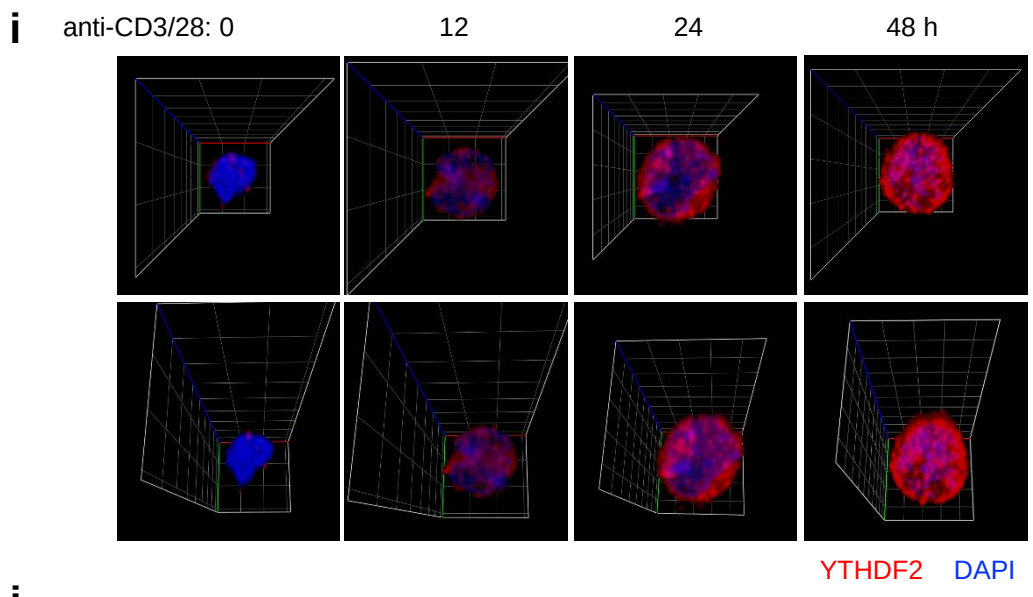
i
anti-CD3/28: 0
12
24
48 h
YTHDF2
DAPI

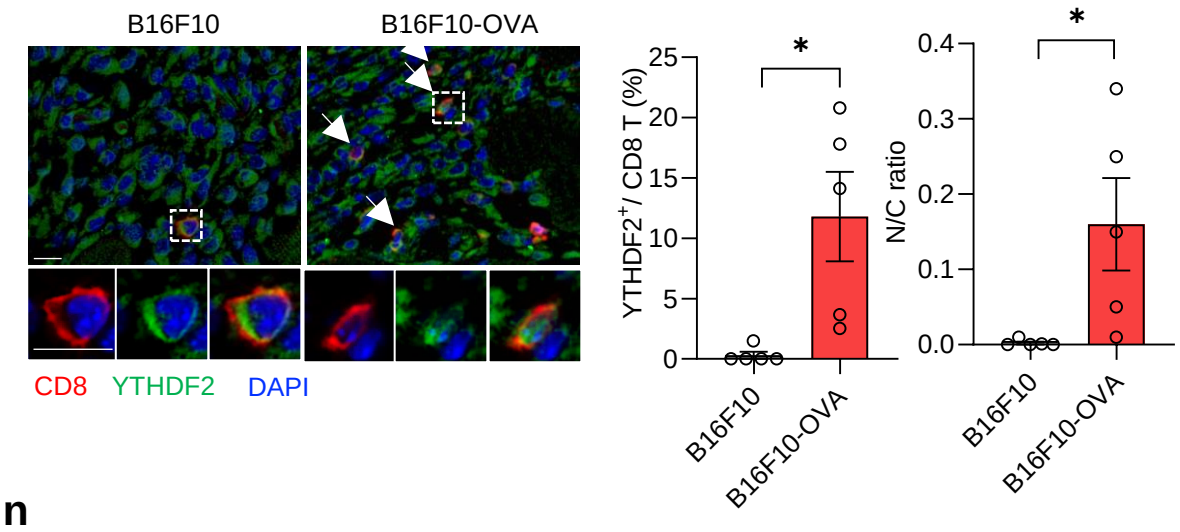
m
B16F10
B16F10-OVA
CD8
YTHDF2
DAPI
YTHDF2+/ CD8 T (%)
25
20
15
10
5
0
*
B16F10
B16F10-OVA
N/C ratio
0.4
0.3
0.2
0.1
0.0
*
B16F10
B16F10-OVA

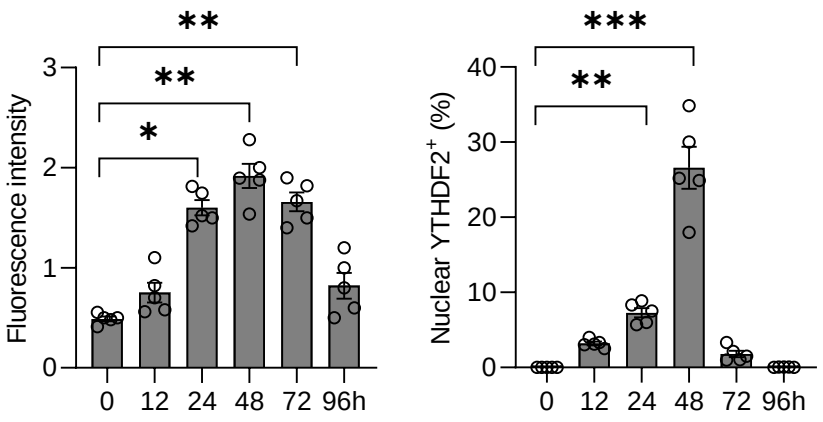
j
Fluorescence intensity
3
2
1
0
**
**
*
0 12 24 48 72 96h
Nuclear YTHDF2+ (%)
40
30
20
10
0
***
**
0 12 24 48 72 96h

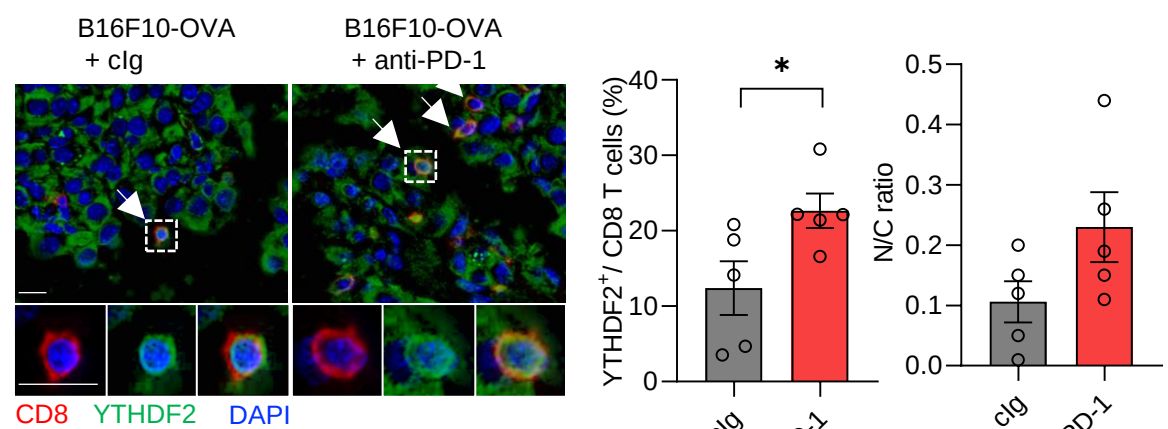
n
B16F10-OVA
+ cIg
B16F10-OVA
+ anti-PD-1
CD8
YTHDF2
DAPI
YTHDF2+/ CD8 T cells (%)
40
30
20
10
0
*
cIg
anti-PD-1
N/C ratio
0.5
0.4
0.3
0.2
0.1
0.0
cIg
anti-PD-1

Supplementary Fig. 1 | YTHDF2 is characteristically expressed upon T cell activation and reinvigoration. a–d mRNA expression of m^{6}A modifiers in naïve or activated mouse T cells. mRNA expression of m^{6}A modifiers in T tolerant (T_{tol}), T helper (T_H1, T_H2 and T_H17), natural regulatory T (nT_{reg}) and naïve T cells (c). mRNA expression of m^{6}A modifiers in OVA-specific CD8 TILs from anti-PD-1- or cIg-treated mouse tumors (d). **e–f** Protein expression of m^{6}A modifiers in human (e) or mouse (f) CD8 T cells primed for the indicated time. **g** LC-MS/MS-based m^{6}A quantification in mRNAs from naïve and activated CD8 T cells (anti-CD3/CD28, 5 μg/ml, 24 h) (n = 3 per group). **h** Metagene distribution of the m^{6}A peaks of naïve and active CD8 T cells along the whole transcriptome. The enriched consensus motifs were detected within m^{6}A peaks. **i** Representative confocal Z-stack images of YTHDF2 (red), and DAPI (blue) in naïve or activated CD8 T cells. **j** Quantification of YTHDF2 intensity of CD8 T cells (left) and frequencies of nuclear YTHDF2$^+$ cells from naïve or activated (right) CD8 T cells (n = 5 per group). **k** Immunoblotting analysis of YTHDF2 in the cytosol and nucleus of Jurkat cells stimulated with or without PHA (150 ng/ml, 24 h). β-actin or Lamin B was used as an internal control. **l** Representative confocal Z-stack images of YTHDF2 (red) and DAPI (blue) in unstimulated Jurkat cells. Scale bar, 10 μm. **m–n** Representative multiplexable immunofluorescent staining of CD8 (red) and YTHDF2 (green) within B16F10 or B16F10-OVA tumors that were grown from OT-1 mice (m) (n = 5 per group) and cIg- or anti-PD-1-treated B16F10-OVA tumors that were grown from wild-type mice (n) (n = 5 per group). A dashed box represents the 4× enlarged area shown in the bottom panels with separate channels. White arrows point to cells positive for YTHDF2 and CD8. Scale bar, 10 μm. Middle panel, frequencies of YTHDF2-positive CD8 T cells. Right panel, quantification of the nuclear to cytoplasmic ratios of YTHDF2 intensity in YTHDF2-positive CD8 T cells. Error bars, mean ± s.e.m. *P < 0.05; **P < 0.01; ***P < 0.001. Two-tailed unpaired Student's t-test (j, m, n).

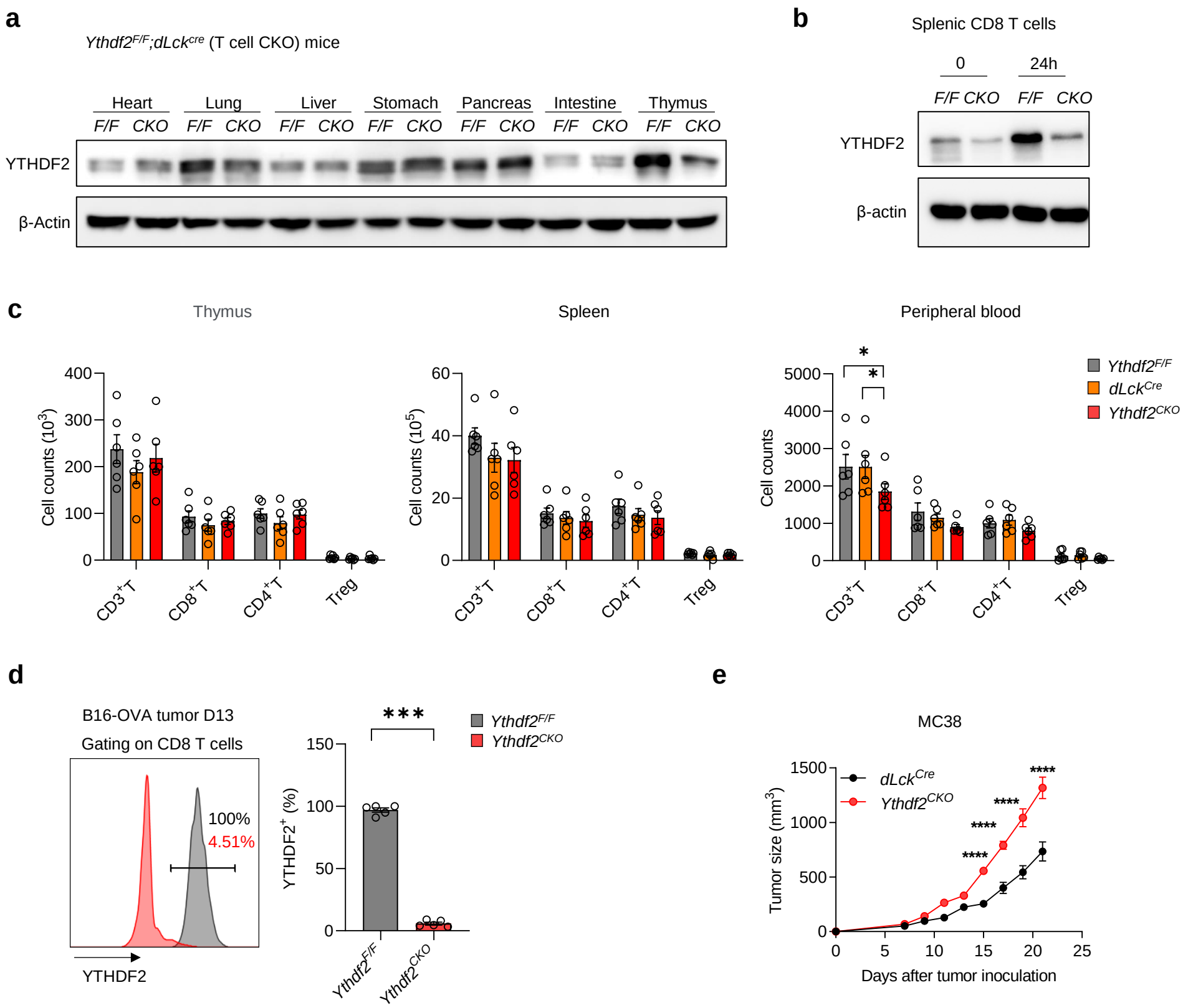

Supplementary Fig. 2 | Phenotyping for the YTHDF2 conditional knockout miceYTHDF2 deprivation hinders antitumor T cell immune response. a Immunoblotting analysis of YTHDF2 expression in heart, lung, liver, stomach, pancreas, intestine and thymus tissues from *Ythdf2*$^{F/F}$ and *Ythdf2*^{CKO} mice. **b** Protein expression of YTHDF2 in naïve and activated CD8 T cells (anti-CD3/CD28, 5 μg/ml, 24 h) derived from *Ythdf2*$^{F/F}$ and *Ythdf2*^{CKO} mouse spleens. **c** Flow cytometry analysis of immune cells within the thymuses, spleens, peripheral blood from *Ythdf2*$^{F/F}$, *dLck*^{Cre} and *Ythdf2*^{CKO} mice (n = 6 per group). **d** Quantification of YTHDF2 expression in B16-OVA tumor-infiltrating CD8 T cells from *Ythdf2*$^{F/F}$ and *Ythdf2*^{CKO} mice (n = 5 per group). **e** Female *dLck*^{Cre} (n = 5) and *Ythdf2*^{CKO} (n = 5) mice were injected subcutaneously with 10^6 MC38 cells. Tumor growth was monitored ever 2 or 3 days. Error bars, mean ± s.e.m. **P* < 0.05; ****P* < 0.001; *****P* < 0.0001. One-way (c) or two-way ANOVA (e) or two-tailed unpaired Student's t-test (d).

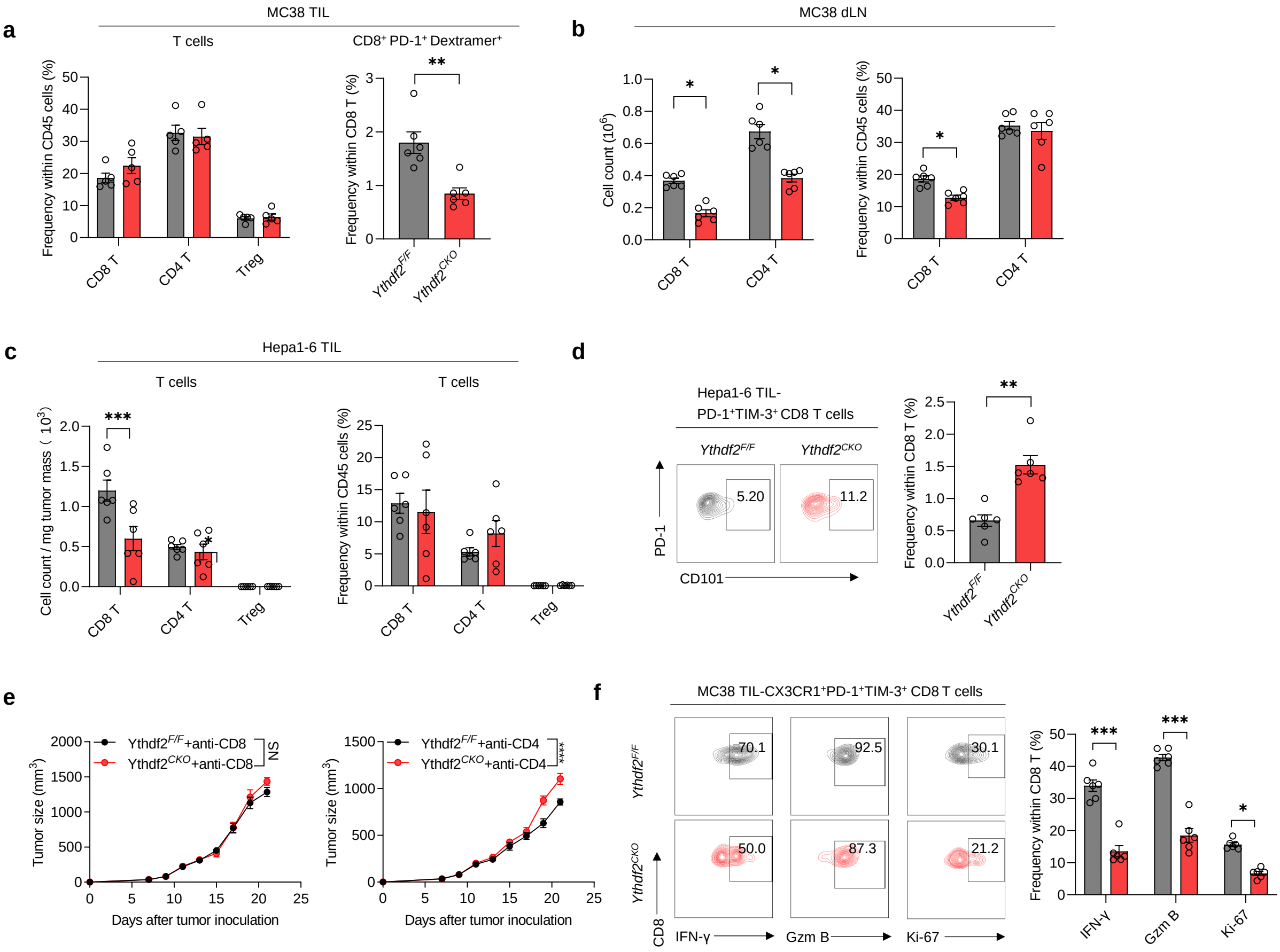

Supplementary Fig. 3 | YTHDF2 deprivation hinders antitumor T cell immune response. a TILs were isolated from *Ythdf2*$^{F/F}$ (n = 5) and *Ythdf2*^{CKO} (n = 5) mice 12 days after MC38 tumor inoculation. Frequencies of immune subsets (CD8 T, CD4 T and T_{reg} cells) within TILs and frequencies of PD-1^{+}KILTFDRL-Dextramer^{+} CD8 T cell subpopulations were assessed by flow cytometry. **b** Numbers and frequencies of immune subsets within tumor-draining lymph nodes (dLN) from MC38 tumor-bearing *Ythdf2*$^{F/F}$ (n = 6) and *Ythdf2*^{CKO} (n = 6) mice. **c** TILs were isolated from *Ythdf2*$^{F/F}$ (n = 6) and *Ythdf2*^{CKO} (n = 6) mice 10 days after Hepa1-6 tumor inoculation. Frequencies of immune subsets (CD8 T, CD4 T and T_{reg} cells) within TILs and frequencies of PD-1^{+}KILTFDRL-Dextramer^{+} CD8 T cell subpopulations were assessed by flow cytometry. **d** Frequencies of PD-1^{+}TIM3^{+}CD101^{+} CD8 T cell subpopulations from Hepa1-6 tumor-bearing *Ythdf2*$^{F/F}$ (n = 6) and *Ythdf2*^{CKO} (n = 6) mice (Day 14). **e** MC38-bearing *Ythdf2*$^{F/F}$ (n = 5) and *Ythdf2*^{CKO} (n = 5) mice were treated with anti-CD8 (200 μg/mouse) (left) or anti-CD4 antibody (200 μg/mouse) (right) and monitored for tumor growth. **f** Frequencies of CX3CR1^{+}Tim3^{+}CD101^{-} CD8 T cell subpopulations positive for Gzm B, IFN-γ or Ki-67 from MC38 tumor-bearing *Ythdf2*$^{F/F}$ (n = 6) and *Ythdf2*^{CKO} (n =6) mice with anti-PD-1 treatment (D12). Error bars, mean ± s.e.m. NS, no significance; **P* < 0.05; ***P* < 0.01; ****P* < 0.001; *****P* < 0.0001. Two-way ANOVA (e) or two-tailed unpaired Student's t-test (a–d, f).

a

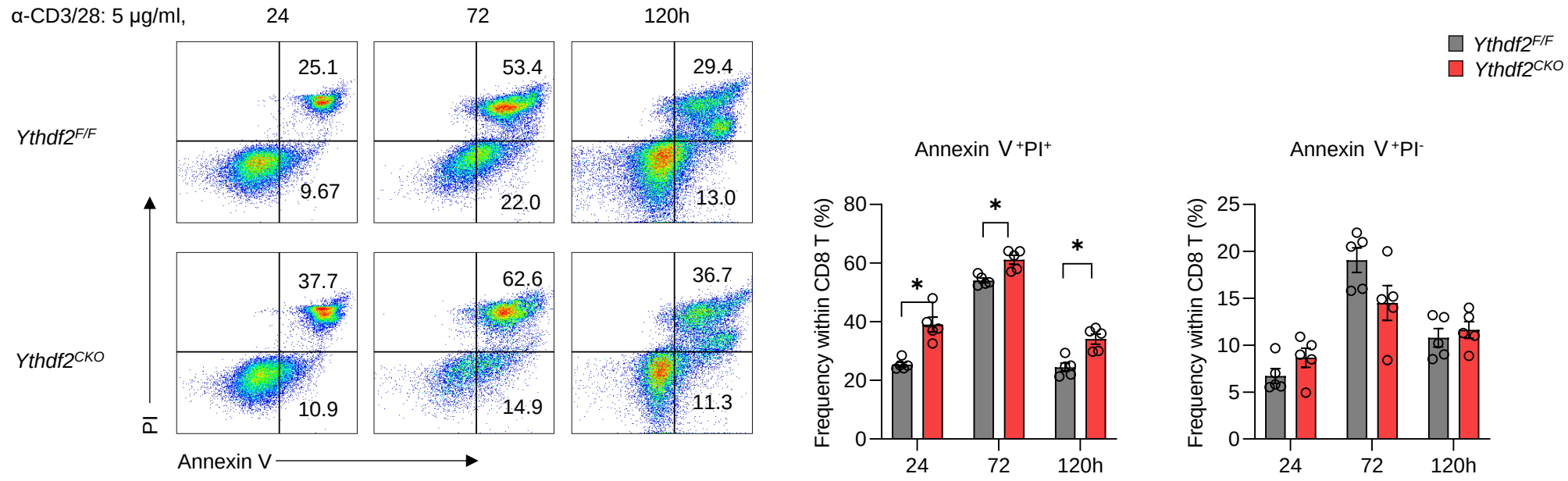
α-CD3/28: 5 μg/ml,
24
72
120h
Ythdf2F/F
Ythdf2CKO
25.1
9.67
53.4
22.0
29.4
13.0
37.7
10.9
62.6
14.9
36.7
11.3
PI
Annexin V
Ythdf2F/F
Ythdf2CKO
Annexin V+PI+
Annexin V+PI-
Frequency within CD8 T (%)
24
72
120h

b

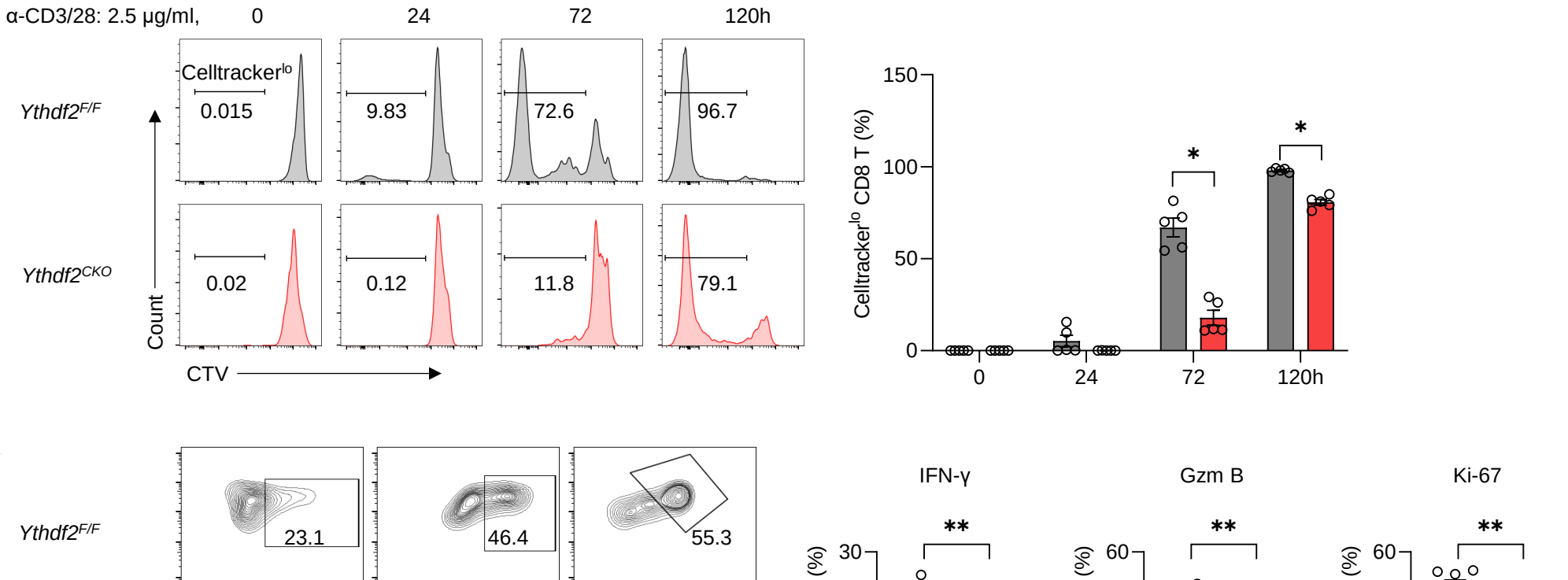
α-CD3/28: 2.5 μg/ml,
0
24
72
120h
Celltrackerlo
0.015
9.83
72.6
96.7
0.02
0.12
11.8
79.1
Count
CTV
Celltrackerlo CD8 T (%)
0
24
72
120h

c

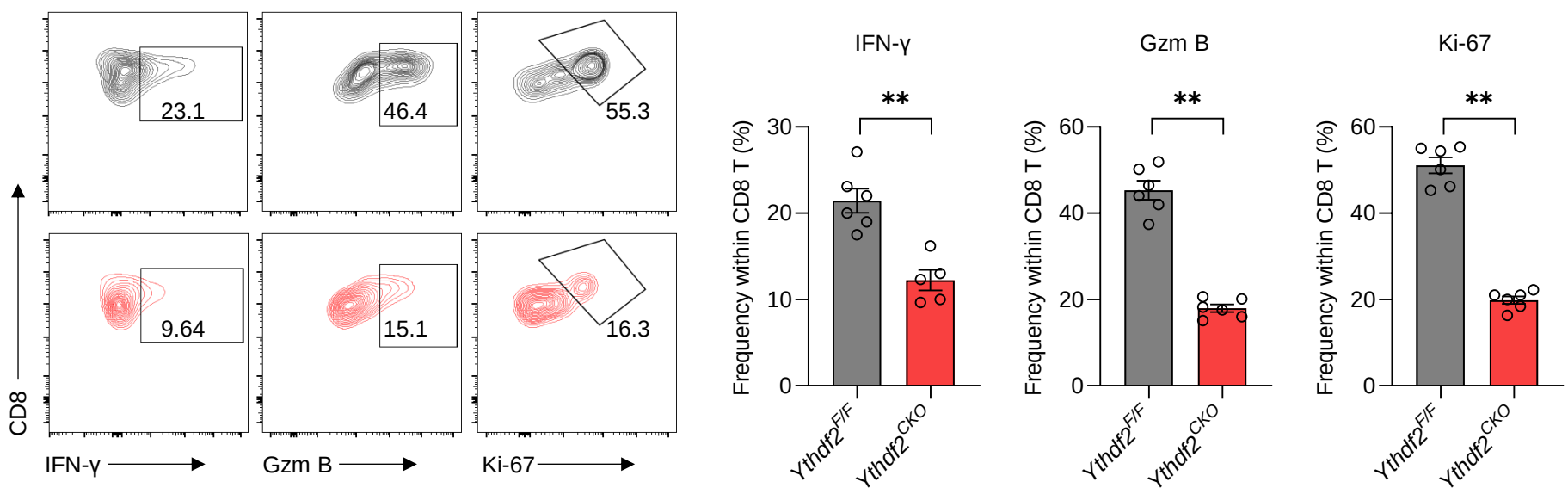
23.1
46.4
55.3
9.64
15.1
16.3
CD8
IFN-γ
Gzm B
Ki-67
IFN-γ
Gzm B
Ki-67
Frequency within CD8 T (%)
Ythdf2F/F
Ythdf2CKO

d

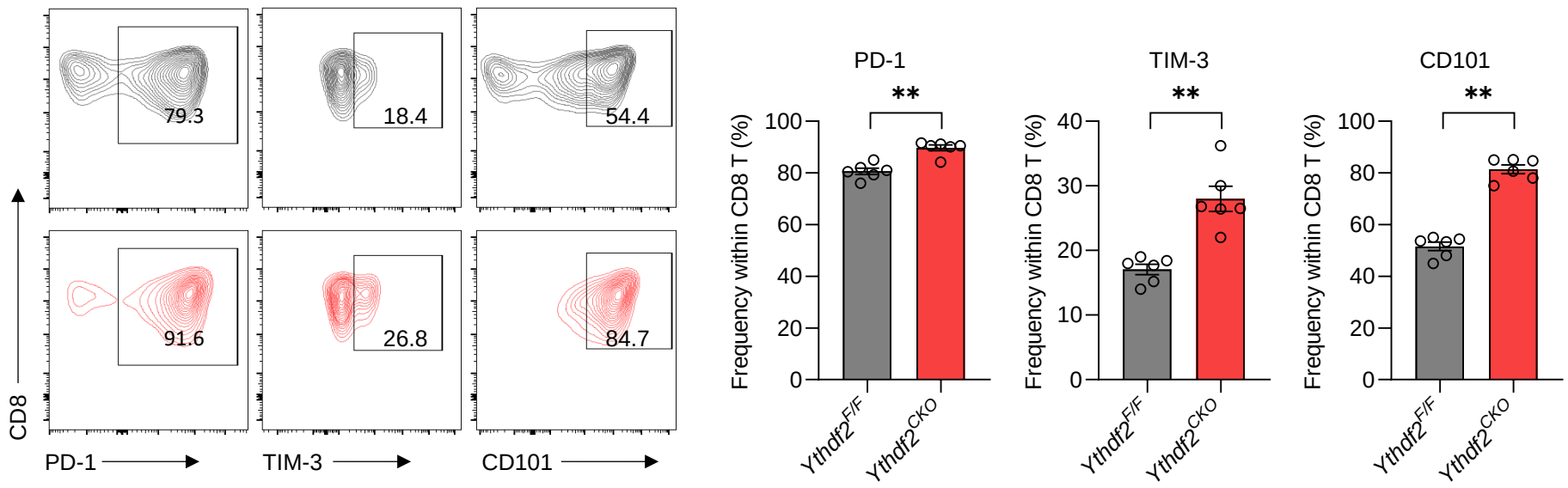
79.3
18.4
54.4
91.6
26.8
84.7
CD8
PD-1
TIM-3
CD101
PD-1
TIM-3
CD101
Frequency within CD8 T (%)
Ythdf2F/F
Ythdf2CKO

e

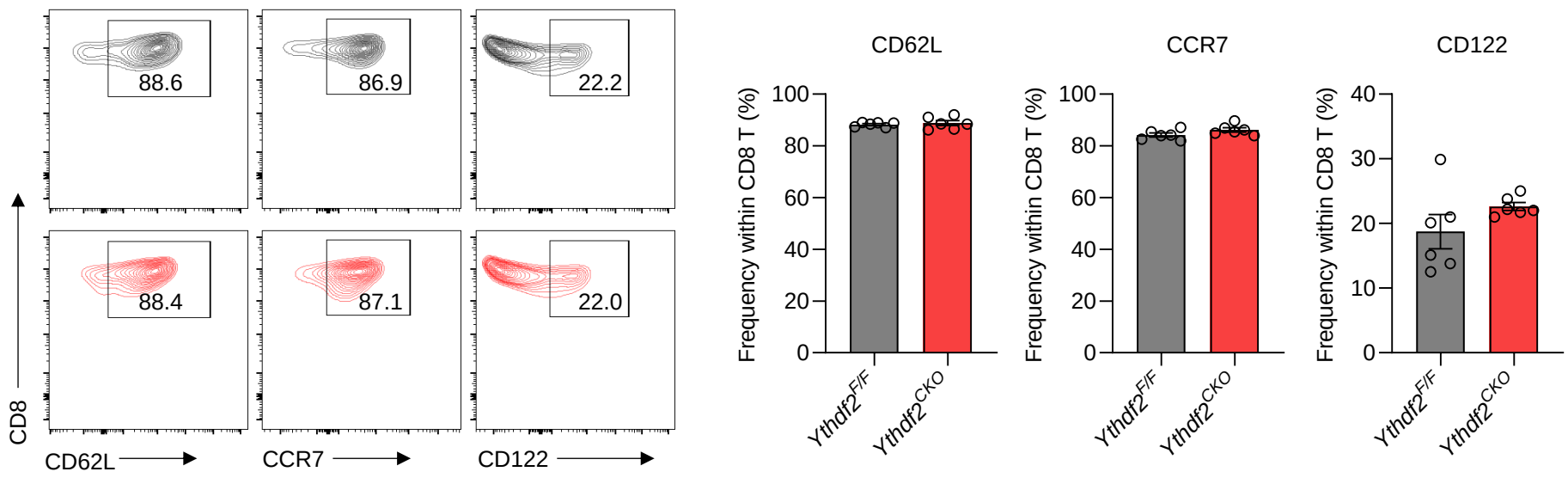
88.6
86.9
22.2
88.4
87.1
22.0
CD8
CD62L
CCR7
CD122
CD62L
CCR7
CD122
Frequency within CD8 T (%)
Ythdf2F/F
Ythdf2CKO

Supplementary Fig. 4 | YTHDF2 maintains CD8 T cell expansion and activation in vitro. a–c Naïve CD8 T cells isolated from *Ythdf2*$^{F/F}$ (n = 5) or *Ythdf2*^{CKO} (n = 5) mice were stimulated with anti-CD3/CD28 (2.5 or 5 μg/ml as indicated) for the indicated time. Apoptosis of *Ythdf2*$^{F/F}$ or *Ythdf2*^{CKO} CD8 T cells was measured by Annexin V and propidium iodide (PI) staining (a). Proliferation of *Ythdf2*$^{F/F}$ or *Ythdf2*^{CKO} CD8 T cells was assessed by Celltracker V (CTV) dilution (b). Quantification of frequencies of IFN-γ^{+}, GZM B^{+}, and Ki-67^{+} subpopulations within activated *Ythdf2*$^{F/F}$ or *Ythdf2*^{CKO} CD8 T cells (c). **d** Naïve CD8 T cells isolated from *Ythdf2*$^{F/F}$ (n = 5) or *Ythdf2*^{CKO} (n = 5) mice to induce T cell exhaustion by chronic stimulation (plates coated with anti-CD3, 5 mg/mL, 8 days). Quantification of frequencies of IFN-γ^{+}, GZM B^{+}, and Ki-67^{+} subpopulations within *Ythdf2*$^{F/F}$ or *Ythdf2*^{CKO} CD8 T cells from in vitro T cell exhaustion assay. **e** Quantification of frequencies of CD62L^{+}, CCR7^{+}, and CD122^{+} subpopulations at Day 9 of transient stimulation (CD3/CD28 beads,1:1 beads-to-cells ratio, 72h) in *Ythdf2*$^{F/F}$ or *Ythdf2*^{CKO} CD8 T cells from in vitro memory-like T cell induction assay (n = 6 per group). Error bars, mean ± s.e.m. **P* < 0.05; ***P* < 0.01. Two-tailed unpaired Student's t-test (a–e).

a

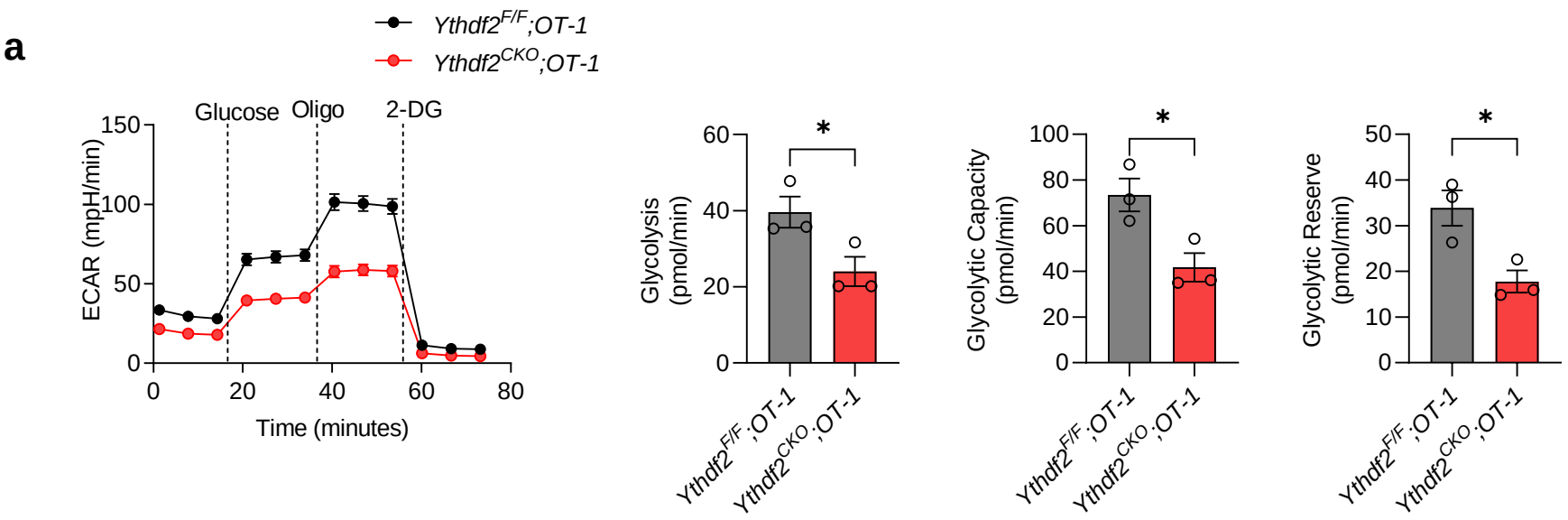
Ythdf2F/F;OT-1
Ythdf2CKO;OT-1
Glucose
Oligo
2-DG
ECAR (mpH/min)
Time (minutes)
Glycolysis (pmol/min)
Glycolytic Capacity (pmol/min)
Glycolytic Reserve (pmol/min)
Ythdf2F/F;OT-1
Ythdf2CKO;OT-1

b

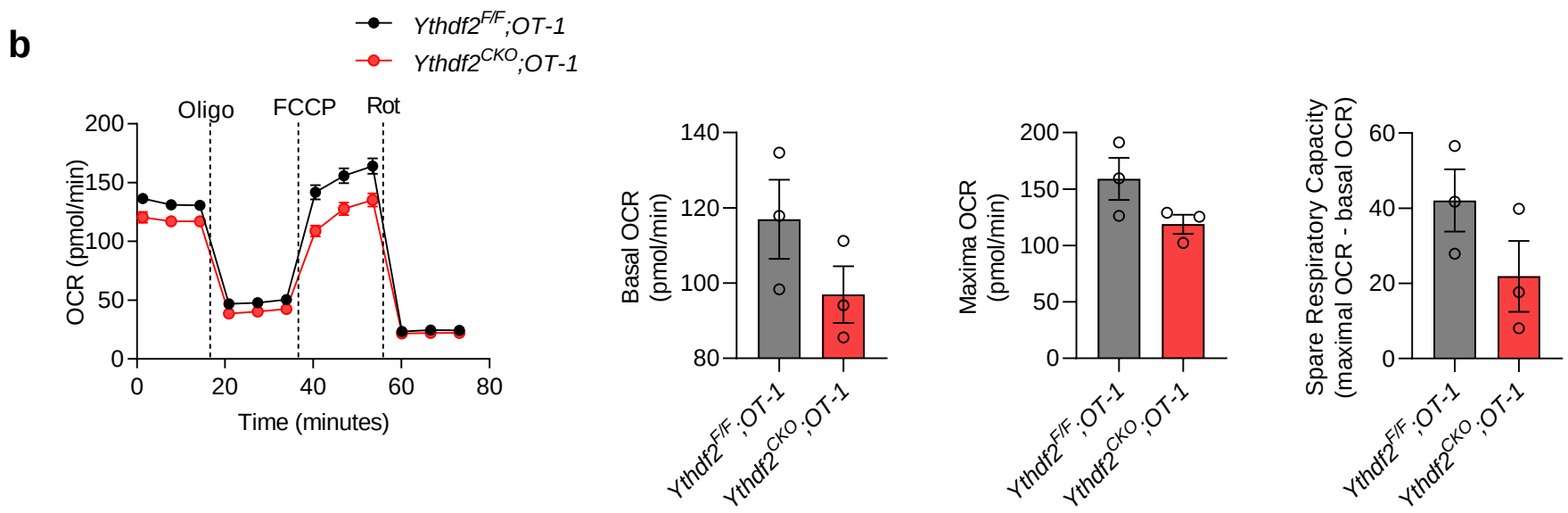
Ythdf2F/F;OT-1
Ythdf2CKO;OT-1
Oligo
FCCP
Rot
OCR (pmol/min)
Time (minutes)
Basal OCR (pmol/min)
Maxima OCR (pmol/min)
Spare Respiratory Capacity (maximal OCR - basal OCR)
Ythdf2F/F;OT-1
Ythdf2CKO;OT-1

c

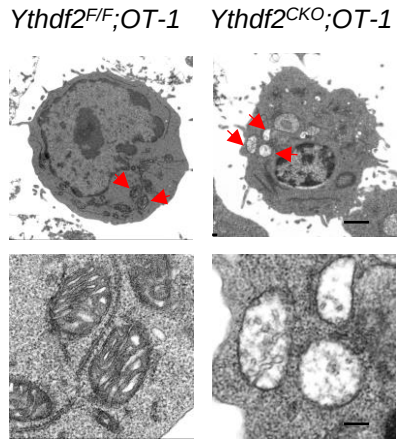
Ythdf2F/F;OT-1
Ythdf2CKO;OT-1

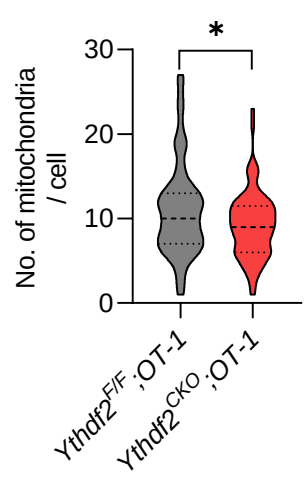
No. of mitochondria / cell
Ythdf2F/F;OT-1
Ythdf2CKO;OT-1

d

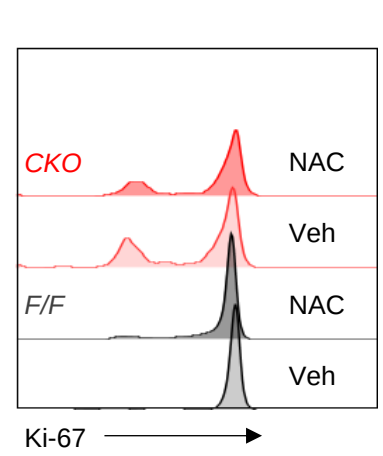
Ki-67
CKO
NAC
Veh
F/F
NAC
Veh
Ki-67

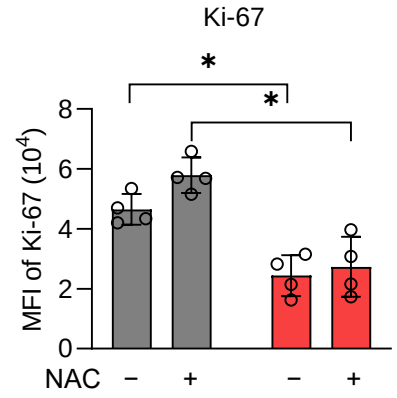
Ki-67
MFI of Ki-67 (10^4)
NAC

e

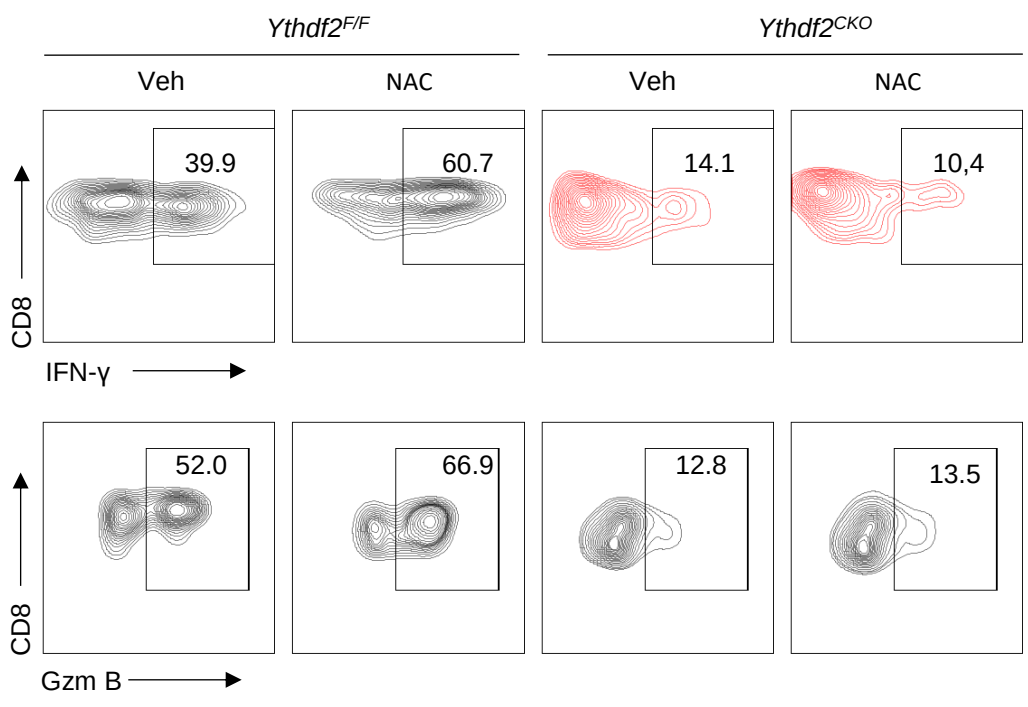
Ythdf2F/F
Ythdf2CKO
Veh
NAC
Veh
NAC
39.9
60.7
14.1
10,4
CD8
IFN-γ
52.0
66.9
12.8
13.5
CD8
Gzm B

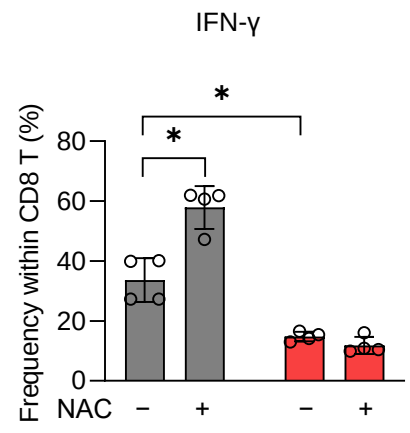
IFN-γ
Frequency within CD8 T (%)
NAC

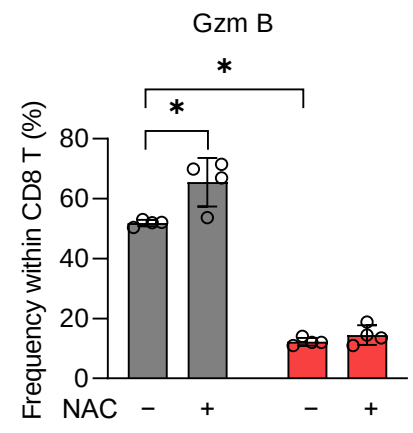
Gzm B
Frequency within CD8 T (%)
NAC

Supplementary Fig. 5 | YTHDF2 deficiency impairs the mitochondria function of CD8 T cells. a–b Extracellular acidification rate (ECAR) levels (a) and oxygen consumption rate (OCAR) levels of primed *Ythdf2*$^{F/F;}$*OT-1* or *Ythdf2*^{CKO}*;OT-1* CD8 T cells (OVA, 10 nM, 72 h) were measured in real-time with Seahorse assay (n = 3 per group). **c** Transmission electron microscopic (TEM) analysis of mitochondrial morphology in activated *Ythdf2*$^{F/F;}$*OT-1* or *Ythdf2*^{CKO}*;OT-1* CD8 T cells (OVA, 10 nM, 72 h). Red arrows in the left panels show the position of mitochondria in respective higher magnification in the right panels. Scale bar, 200 nm. **d–e** Quantification of Ki-67 MFI (d), IFN-γ^{+}, GZM B^{+} (e) frequencies among *Ythdf2*$^{F/F}$ and *Ythdf2*^{CKO} CD8 T cells primed in the T cell exhaustion assay (plates coated with anti-CD3, 5 mg/mL, 8 days) with 10 mM NAC or veh (72 h) (n = 4 per group). For the violin plots, the plots are centered around the median, extending from the 25th to the 75th percentiles, while the whiskers represent the minimum and maximum values(c). Error bars, mean ± s.e.m. **P* < 0.05. Two-tailed unpaired Student's t-test (a–c). Two-way ANOVA (d, e).

a

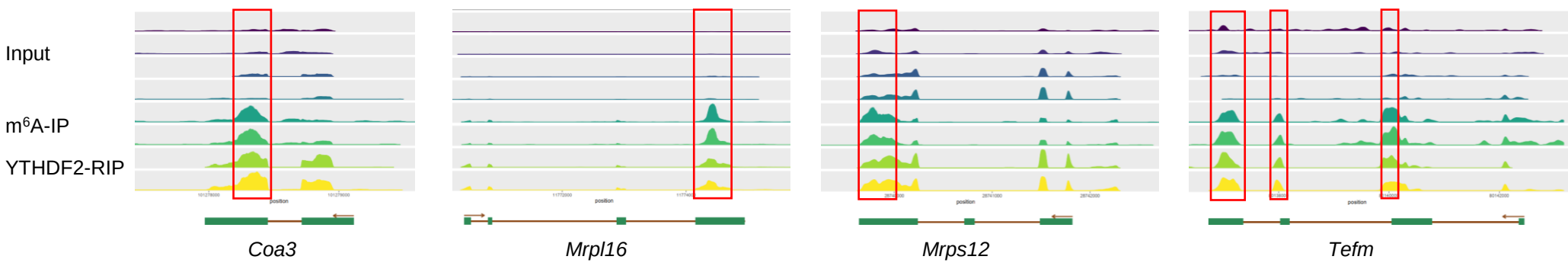

b

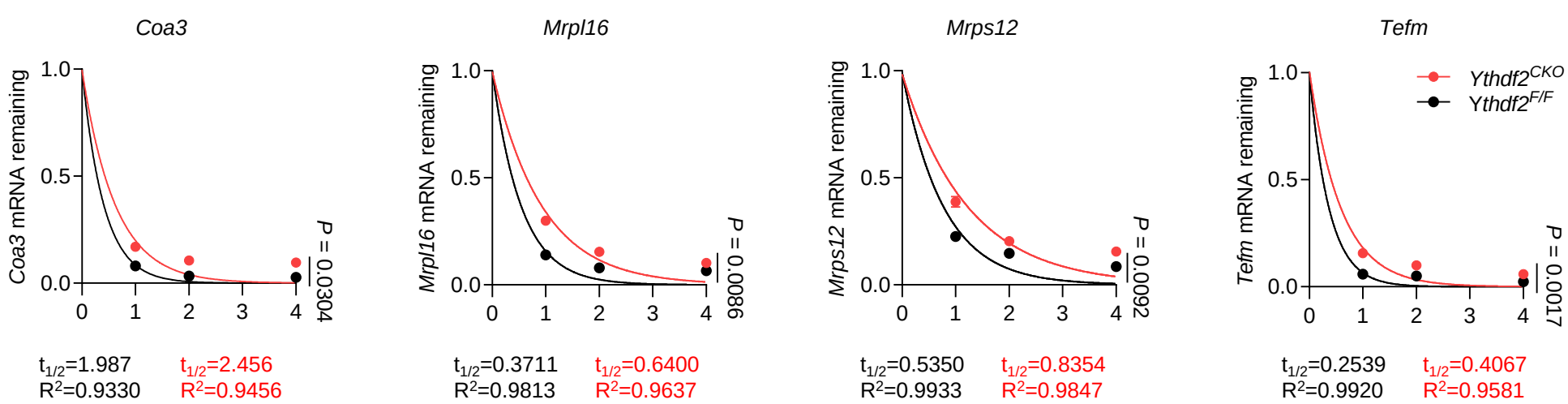

c

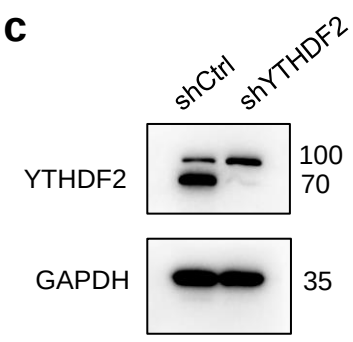

d

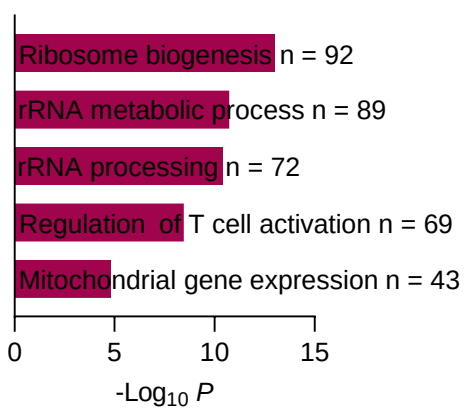

e

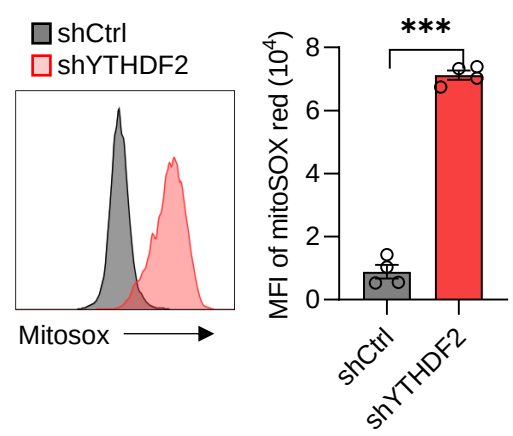

f

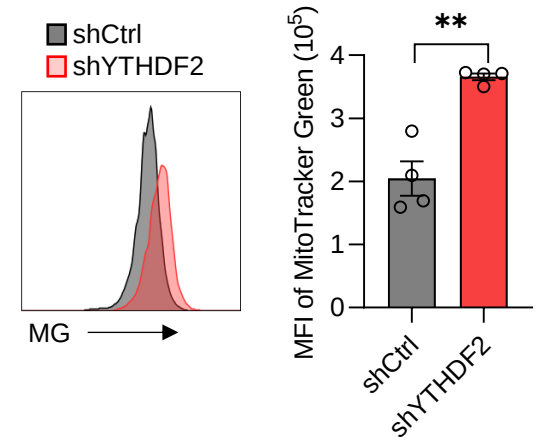

g

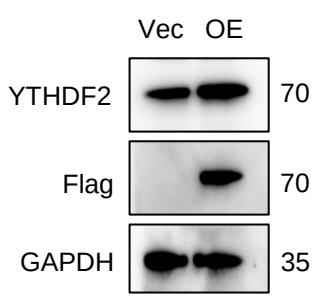

h

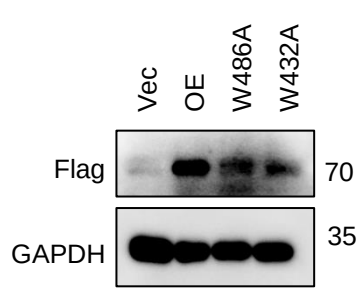

i

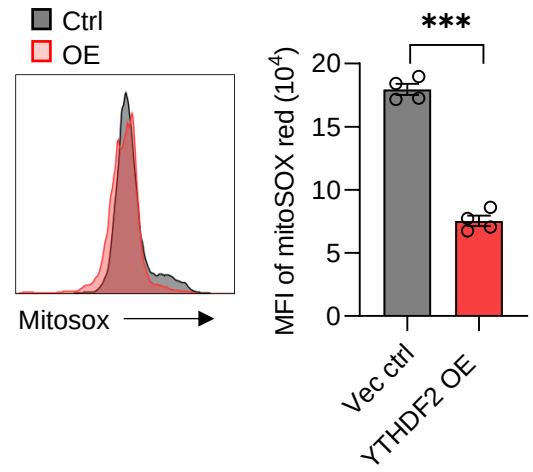

j

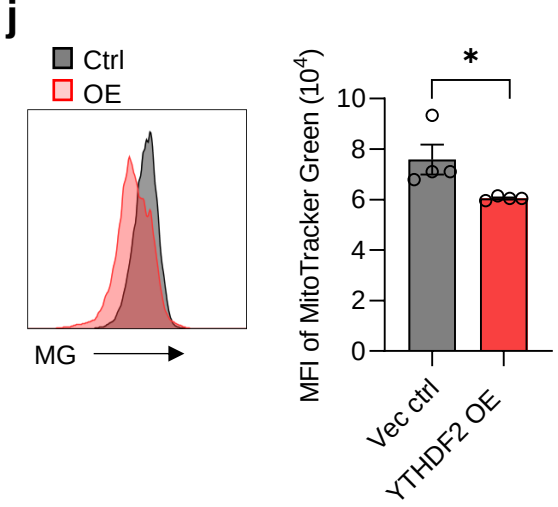

k

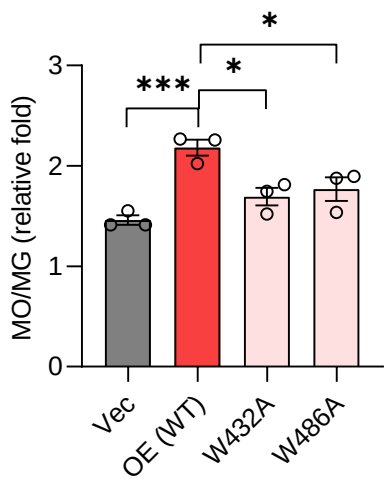

l

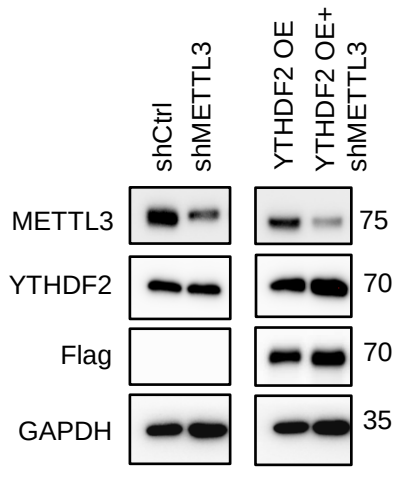

m

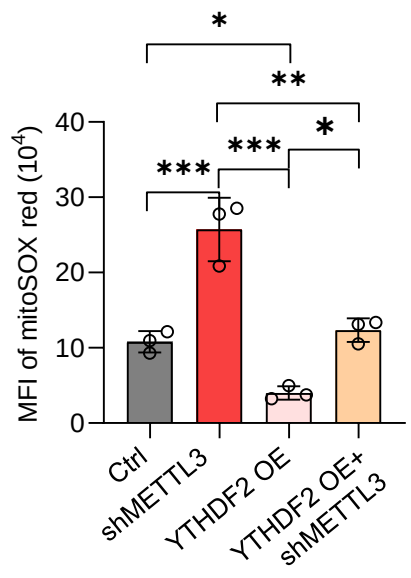

n

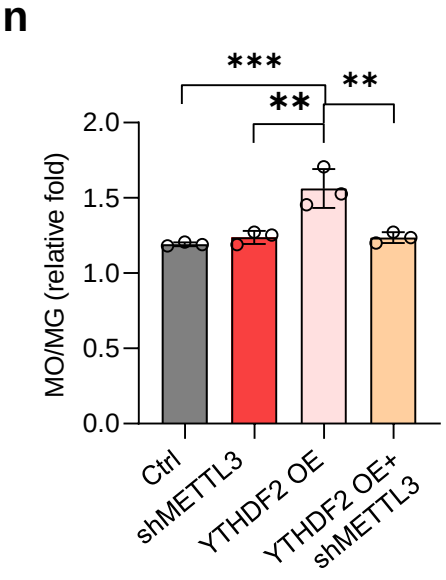

Supplementary Fig. 6 | The m^{6}A machinery is necessary for YTHDF2-regulated mitochondrial fitness. a m^{6}A-seq and RIP-seq tracks of *Coa3, Mrpl16, Mrps12* and *Tefm* mRNA loci on primed*Ythdf2*$^{F/F}$ and *Ythdf2*^{CKO} CD8 T cells. **b** Activated *Ythdf2*$^{F/F}$ and *Ythdf2*^{CKO} CD8 T cells (anti-CD3/CD28, 5 μg/ml, 24 h) were treated with ActD (500 μg/ml) and RNAs were collected at different time points. *Coa3, Mrpl16, Mrps12 and Tefm* mRNA levels were measured using qPCR and represented as mRNA remaining after ActD treatment (n = 3 per group). **c** Immunoblotting analysis of YTHDF2 expression in Jurkat-shCtrl and Jurkat-shYTHDF2 cells. **d** GO enrichment analysis of upregulated genes in Jurkat-shCtrl and Jurkat-shYTHDF2 cells. **e–f** Quantification of MitoSOX (e) and MG (f) MFI in Jurkat-shCtrl and Jurkat-shYTHDF2 cells (n = 4 per group). **g** Immunoblotting analysis of YTHDF2 and Flag expression in Jurkat cells with or without YTHDF2 overexpression (OE) (n = 4 per group). **h** Immunoblotting analysis of Flag expression in Jurkat cells transduced with wild-type (OE) or mutant YTHDF2 (W432A and W486A) or empty vector lentiviruses. **i–j** Quantification of MitoSOX (i) and MG (j) MFI in Jurkat cells with or without YTHDF2 OE (n = 4 per group). **k** Quantification of the MO/MG ratio in Jurkat cells transduced with wild-type or mutant YTHDF2 or empty vector lentiviruses (n = 3 per group). **l** Immunoblotting analysis of METTL3, YTHDF2 and Flag expression in YTHDF2-OE Jurkat cells with or without knockdown of METTL3. **m** MitoSOX staining among METTL3-knockdown and control Jurkat cells with or without YTHDF2 overexpression (n = 3 per group). **n** Quantification of the MO/MG ratio among METTL3-knockdown and control Jurkat cells with or without YTHDF2 overexpression (n = 3 per group). Error bars, mean ± s.e.m. **P* < 0.05; ***P* < 0.01; ****P* < 0.001. Two-tailed unpaired Student's t-test (f, i, j) or one-way ANOVA (k, m, n) or non-linear regression (b).

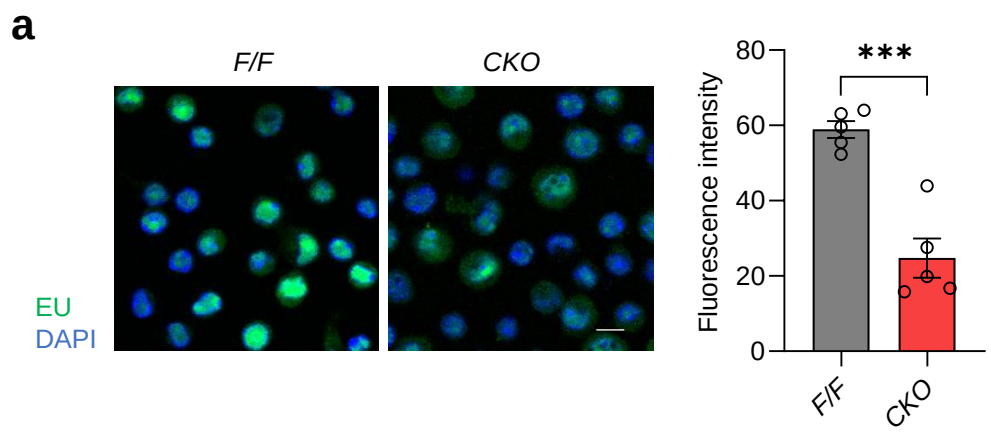

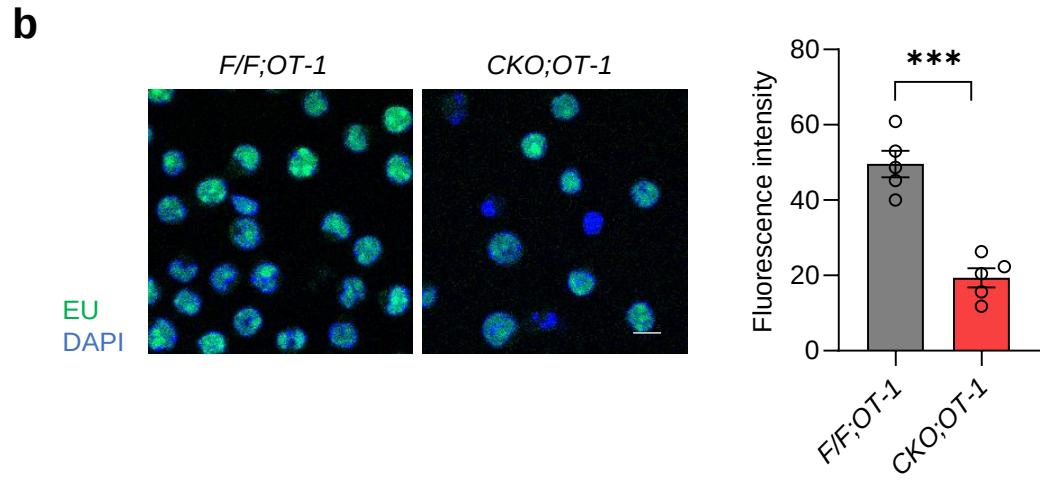

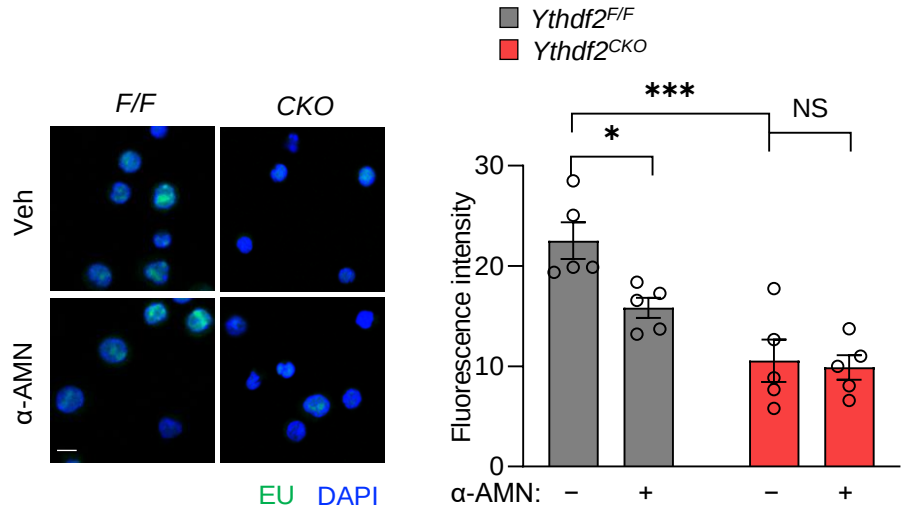

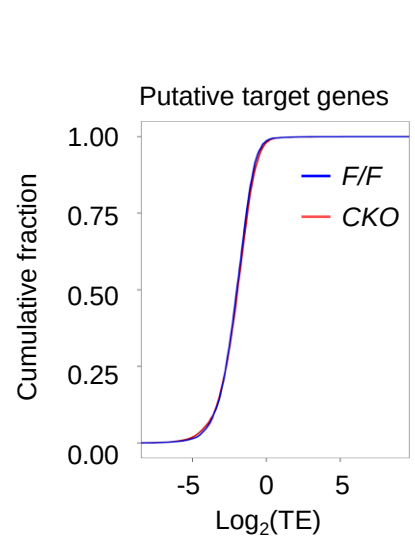

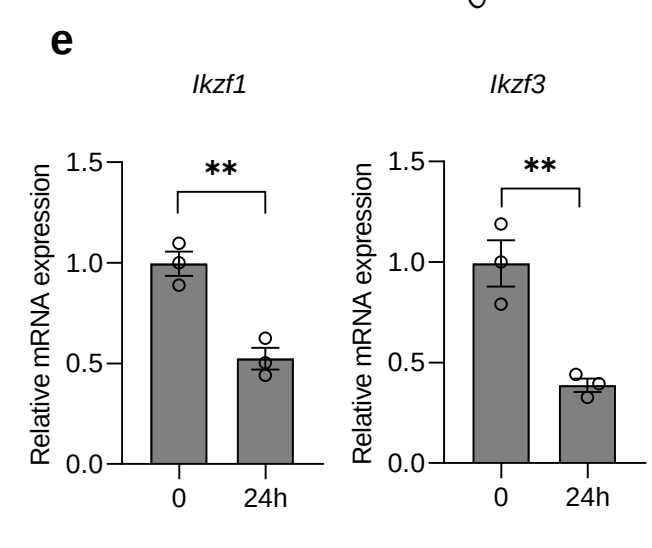

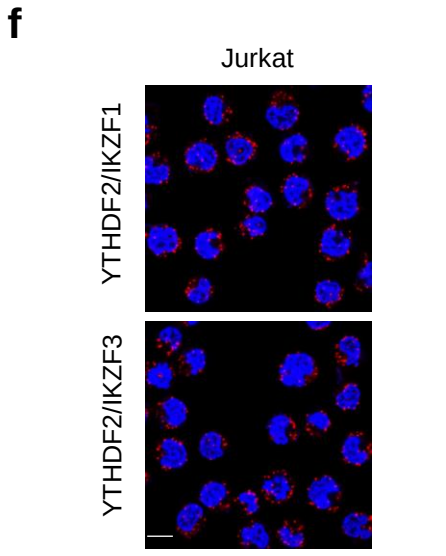

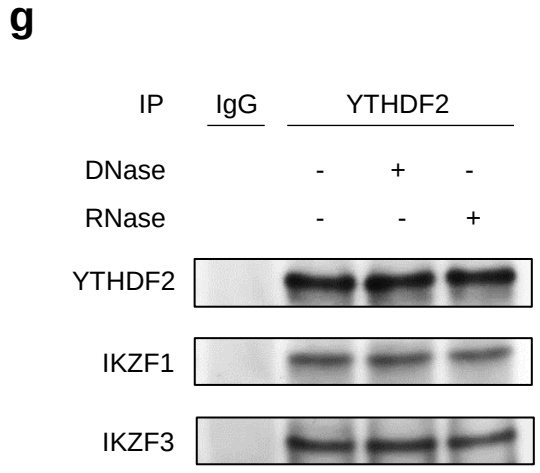

h

Rank	Motif	P-value	log P-pvalue	% of Targets	% of Background
1		1e-1743	-4.016e+03	6.48%	0.50%
2		1e-1042	-2.399e+03	20.60%	8.81%
3		1e-464	-1.069e+03	20.55%	12.06%
4		1e-401	-9.236e+02	6.39%	2.32%
5		1e-248	-5.729e+02	16.32%	10.55%

i

Rank	Motif	P-value	log P-pvalue	% of Targets	% of Background
1		1e-1186	-2.733e+03	36.04%	9.32%
2		1e-685	-1.577e+03	32.62%	11.70%
3		1e-198	-4.567e+02	28.98%	17.00%
4		1e-169	-3.904e+02	26.14%	15.47%
5		1e-132	-3.051e+02	17.70%	9.81%

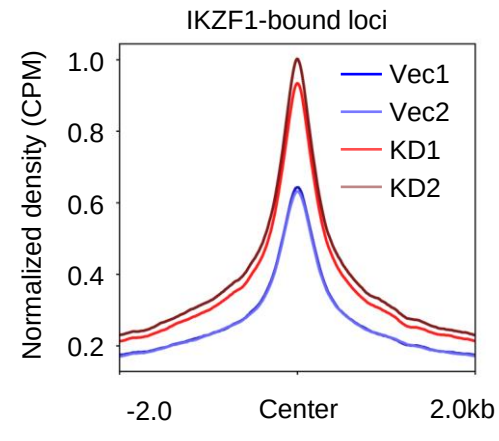

Supplementary Fig. 7 | Acute T cell activation enlists nuclear functionality of YTHDF2. a–b Click-it RNA imaging and analysis of nascent RNA (green) synthesis in activated *Ythdf2*$^{F/F}$ or *Ythdf2*^{CKO} CD8 T cells (anti-CD3/CD28, 5 μg/ml, 24 h) (a) and activated *Ythdf2*$^{F/F;}$*OT-1* or *Ythdf2*^{CKO}*;OT-1* CD8 T cells (OVA, 10 nM, 24 h) (b). Scale bar, 10 μm. **c** Click-it RNA imaging and analysis of nascent RNA (green) synthesis in activated *Ythdf2*$^{F/F}$ or *Ythdf2*^{CKO} CD8 T cells (anti-CD3/CD28, 5 μg/ml, 24 h) in the presence of α-amanitin (2μg/mL, 12 h) or vehicle (n = 5 per group). Scale bar, 10 μm. **d** Cumulative distribution of the fold change in translational efficiency of YTHDF2-targeted and m^{6}A-marked transcripts between activated *Ythdf2*$^{F/F}$ and *Ythdf2*^{CKO} CD8 T cells (anti-CD3/CD28, 5 μg/ml, 24 h). **e** *Ikzf1 and Ikzf3* mRNA levels detected by qPCR in naïve or activated (anti-CD3/CD28, 5 μg/ml, 24 h) CD8 T cells (n = 3 per group). **f** PLA analysis of YTHDF2 associated with IKZF1 or IKZF3 in unstimulated Jurkat cells. Scale bar, 10 μm. **g** Whole-cell lysates of activated WT CD8 T cells (anti-CD3/CD28, 5 μg/ml, 24 h) were subjected to immunoprecipitation using anti-YTHDF2 antibody. The immunoprecipitants were incubated with RNase A (1 ug/ul) or DNase I (0.4 U/ul) DNase followed by immunoblot analysis. **h–i** Motif discovery analysis of the genomic sequences under ATAC-seq peaks conditioned by YTHDF2 depletion using HOMER. Red rectangle shows the IKZF1/3-binding motif within ATAC-sequenced *Ythdf2*$^{F/F}$ and *Ythdf2*^{CKO} CD8 T cells (h) or Jurkat-shCtrl and Jurkat-shYTHDF2 cells (i). **j** ChIP-seq datasets for IKZF1 (GSM935442) in human T cells were obtained using Cistrome Data Browser. ATAC-seq profiles of Jurkat-shCtrl and Jurkat-shYthdf2 cells were represented on IKZF1-bound loci. Error bars, mean ± s.e.m. **P* < 0.05; ***P* < 0.01; ****P* < 0.001. Two-tailed unpaired Student's t-test (a, b, e) or two-way ANOVA (c).

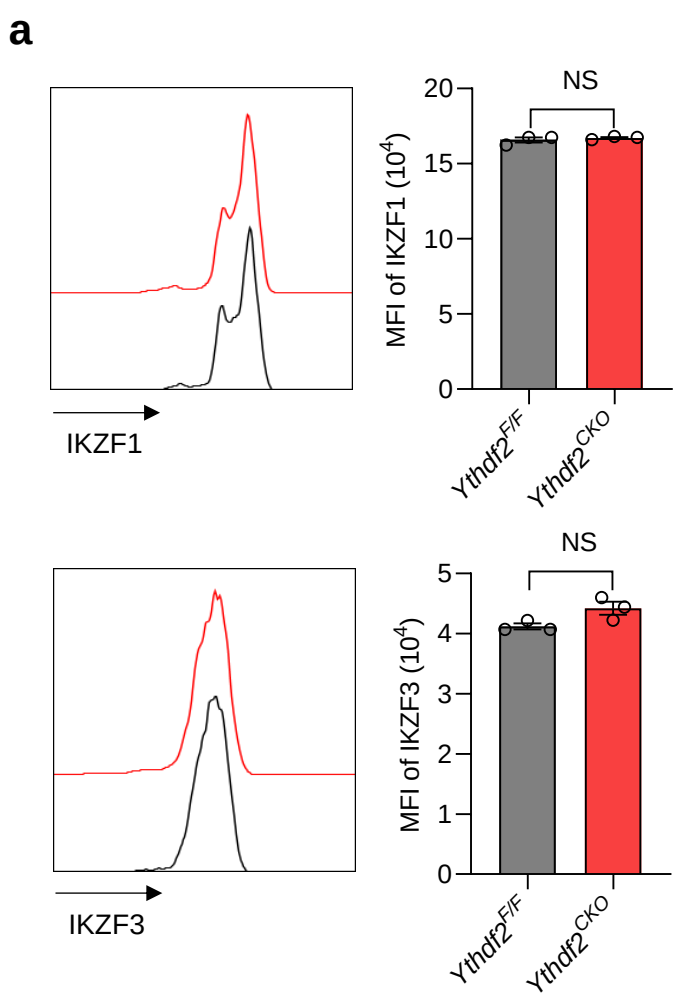
a
IKZF1
MFI of IKZF1 (10^4)
NS
$Ythdf2^{F/F}$
$Ythdf2^{CKO}$
IKZF3
MFI of IKZF3 (10^4)
NS
$Ythdf2^{F/F}$
$Ythdf2^{CKO}$

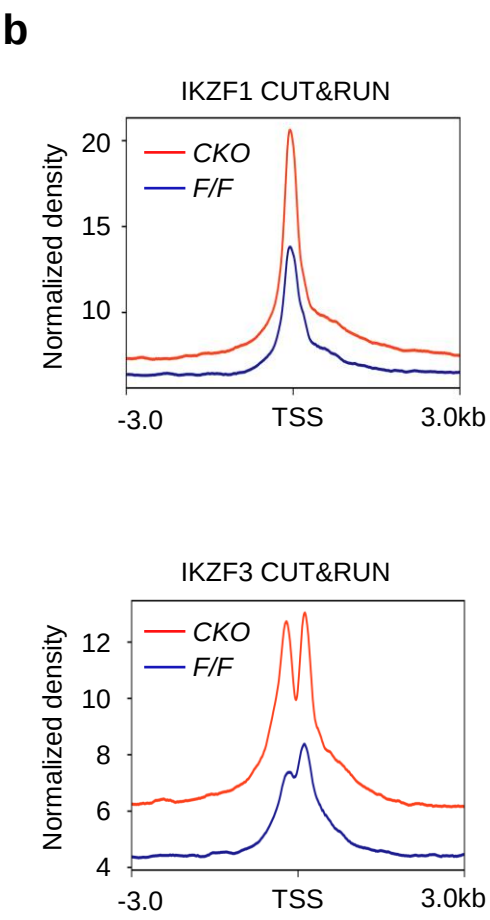
b
IKZF1 CUT&RUN
Normalized density
CKO
F/F
-3.0
TSS
3.0kb
IKZF3 CUT&RUN
Normalized density
CKO
F/F
-3.0
TSS
3.0kb

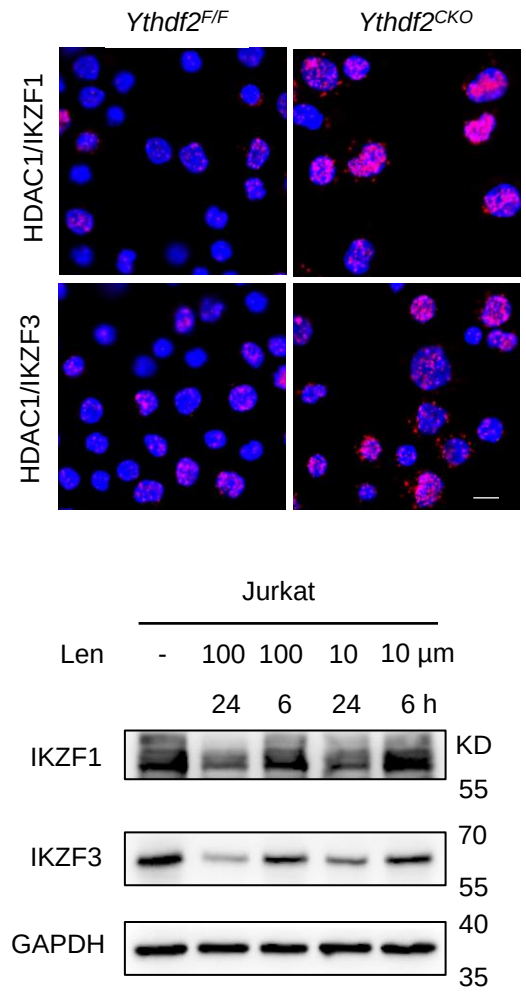
c
$Ythdf2^{F/F}$
$Ythdf2^{CKO}$
HDAC1/IKZF1
HDAC1/IKZF3
e
Jurkat
Len
- 100 100 10 10 μm
24 6 24 6 h
IKZF1
IKZF3
GAPDH
KD
55
70
55
40
35

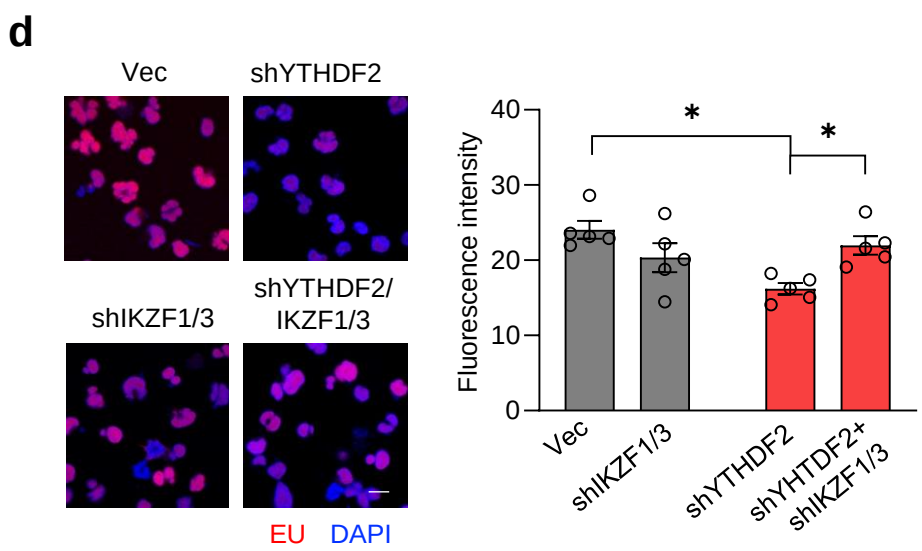
d
Vec
shYTHDF2
shIKZF1/3
shYTHDF2/
IKZF1/3
EU DAPI
Fluorescence intensity
Vec
shIKZF1/3
shYTHDF2
shYHTDF2+
shIKZF1/3

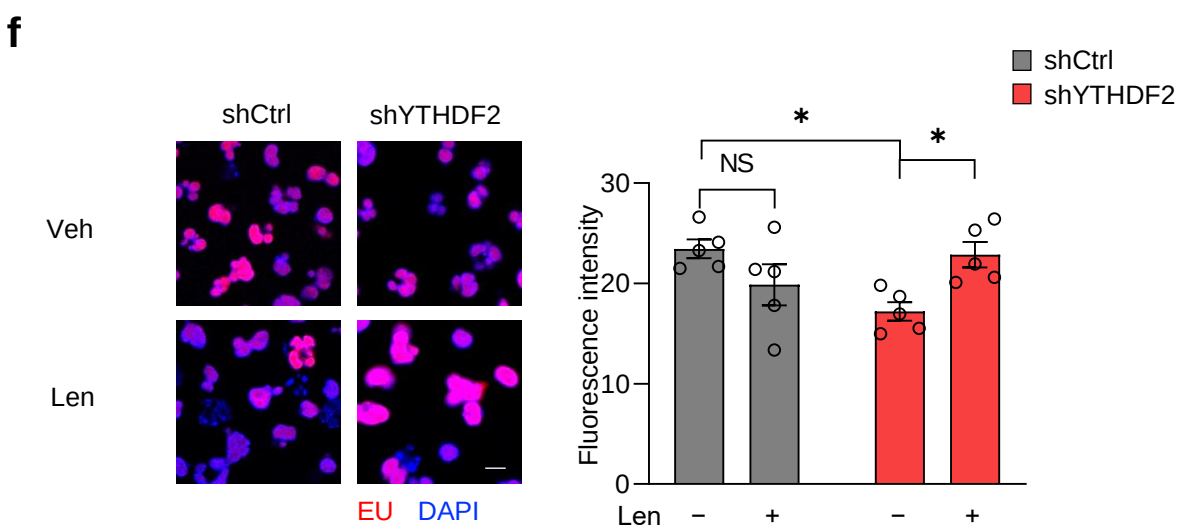
f
shCtrl
shYTHDF2
Veh
Len
EU DAPI
shCtrl
shYTHDF2
NS
Fluorescence intensity
Len

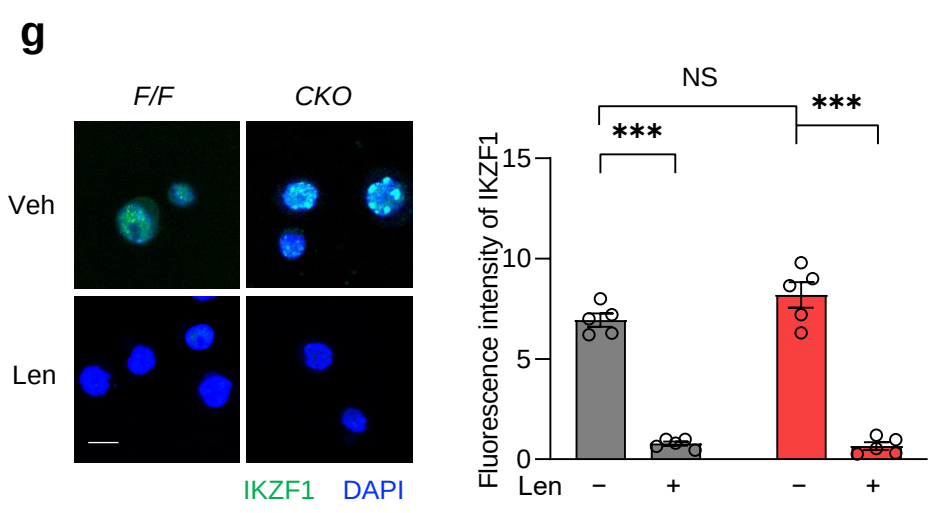
g
F/F
CKO
Veh
Len
IKZF1 DAPI
NS
Fluorescence intensity of IKZF1
Len

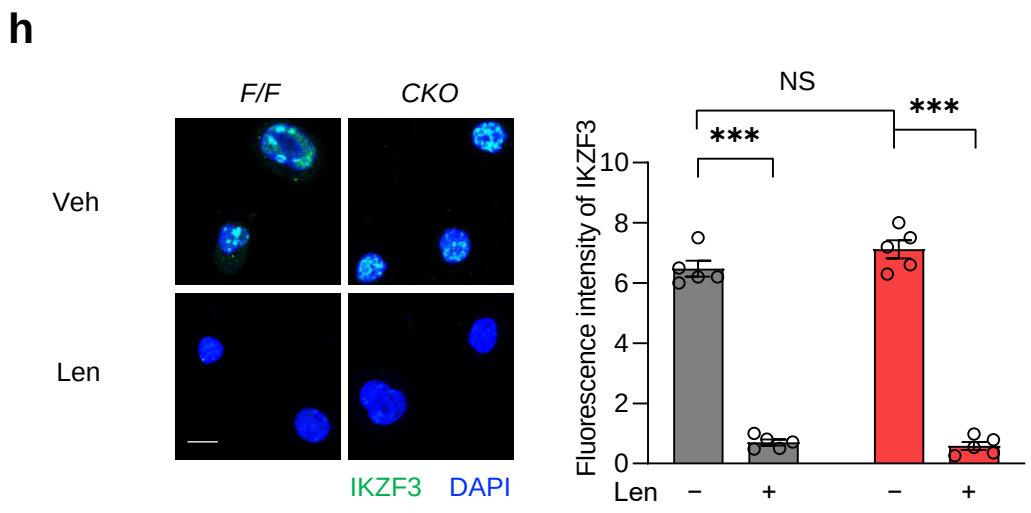
h
F/F
CKO
Veh
Len
IKZF3 DAPI
NS
Fluorescence intensity of IKZF3
Len

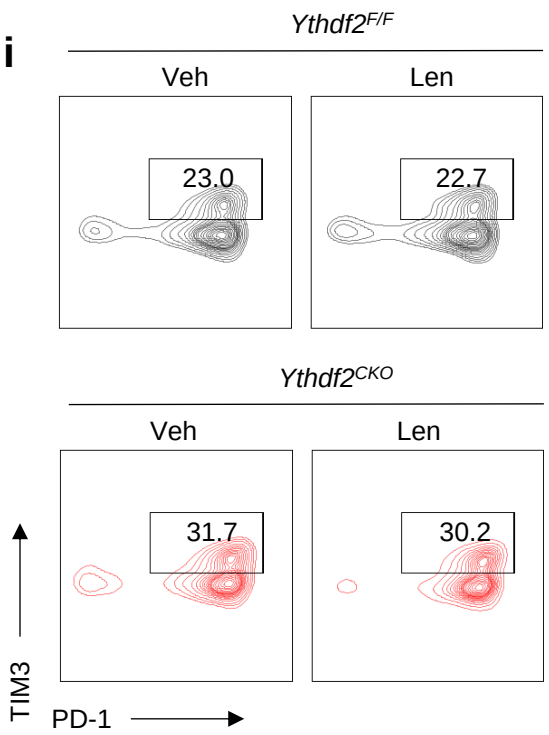
i
$Ythdf2^{F/F}$
Veh
Len
23.0
22.7
$Ythdf2^{CKO}$
Veh
Len
31.7
30.2
TIM3
PD-1

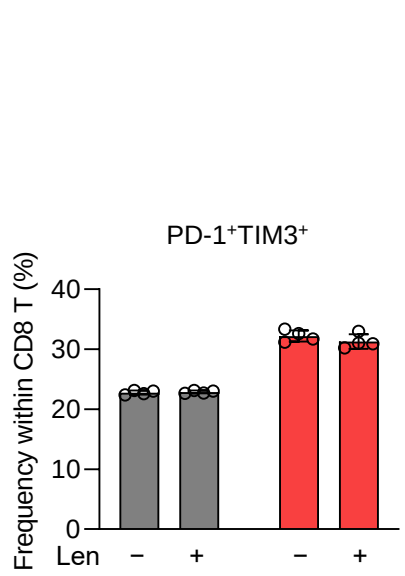
j
PD-1+TIM3+
Frequency within CD8 T (%)
Len

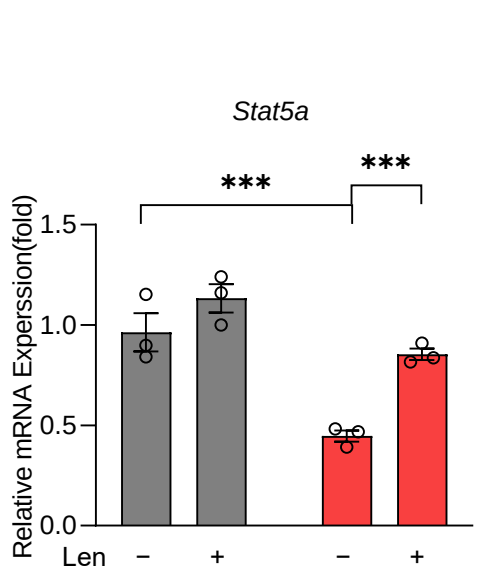
Stat5a
Relative mRNA Expression(fold)
Len

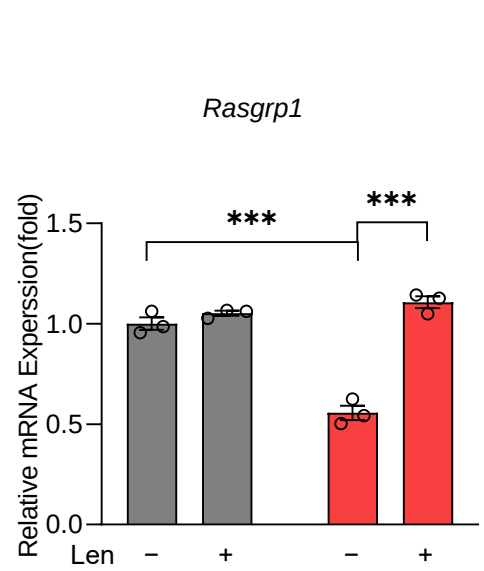
Rasgrp1
Relative mRNA Expression(fold)
Len

Supplementary Fig. 8 | IKZF1/3-associated transcriptional repression in YTHDF2-deficient T cells. **a** Quantitative flow cytometry analysis of IKZF1 (top) or IKZF3 (bottom) expression in activated *Ythdf2*$^{F/F}$ and *Ythdf2*^{CKO} CD8 T cells (anti-CD3/CD28, 5 μg/ml, 24 h) (n = 3). **b** IKZF1 (top) or IKZF3 (bottom) CUT&RUN profiles of activated *Ythdf2*$^{F/F}$ and *Ythdf2*^{CKO} CD8 T cells (anti-CD3/CD28, 5 μg/ml, 24 h) were represented at the gene promoter regions. **c** PLA analysis of HDAC1 associated with IKZF1 or IKZF3 in activated *Ythdf2*$^{F/F}$ and *Ythdf2*^{CKO} CD8 T cells (anti-CD3/CD28, 5 μg/ml, 24 h). Scale bar, 10 μm. **d** Click-it RNA imaging and analysis of nascent RNA synthesis (red) in Jurkat-shCtrl, Jurkat-shIKZF1/3 cells, Jurkat-shYTHDF2 cells and Jurkat-shYTHDF2/IKZF1/3 cells (n = 5 per group). **e** Immunoblotting analyses of IKZF1 and IKZF3 in Jurkat cells treated with len (10 or 100 μM) or veh for 6 or 24 h. **f** Click-it RNA imaging and analysis of nascent RNA synthesis (red) in Jurkat-shCtrl and Jurkat-shYTHDF2 cells in the presence of 100 μM len or veh for 24 h (n = 5 per group). **g**–**h** Representative confocal immunofluorescence images of IKZF1 (g) or IKZF3 (h) (green) and DAPI (blue) in activated *Ythdf2*$^{F/F}$ and *Ythdf2*^{CKO} CD8 T cells (anti-CD3/CD28, 5 μg/ml, 24 h) in the presence of 10 μM len or veh (n = 5 per group). Scale bar, 10 μm. **i** Quantification of Tim3^{+} PD-1^{+} frequencies among primed*Ythdf2*$^{F/F}$ and *Ythdf2*^{CKO} CD8 T cells (anti-CD3/CD28, 5 μg/ml, 48 h) in the presence of 10 μM len or veh (n = 4 per group). **j** *Stat5a* (left) and *Rasgrp1* (right) mRNA levels detected by qPCR in activated *Ythdf2*$^{F/F}$ and *Ythdf2*^{CKO} CD8 T cells (anti-CD3/CD28, 5 μg/ml, 24 h) in the presence of 10 μM len or veh (n = 3 per group). Error bars, mean ± s.e.m. **P* < 0.05; ***P* < 0.01; ****P* < 0.001. Two-tailed unpaired Student's t-test (a). One (d) or two-way (f–j) ANOVA.

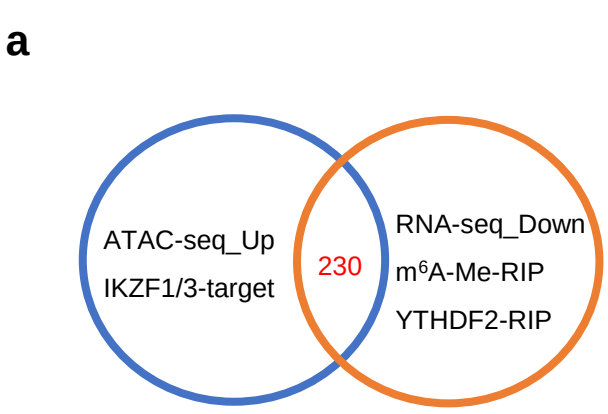
a
ATAC-seq_Up
IKZF1/3-target
230
RNA-seq_Down
m6A-Me-RIP
YTHDF2-RIP

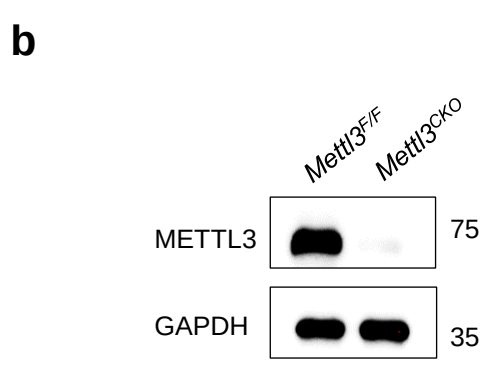
b
Mettl3F/F
Mettl3CKO
METTL3
GAPDH
75
35

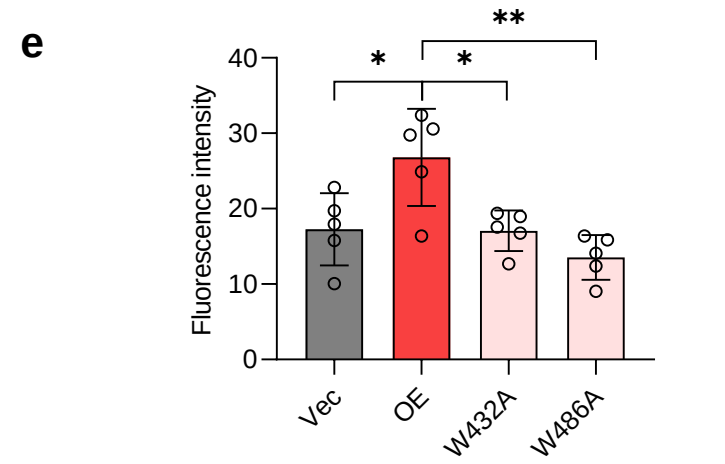
e
Fluorescence intensity
Vec
OE
W432A
W486A

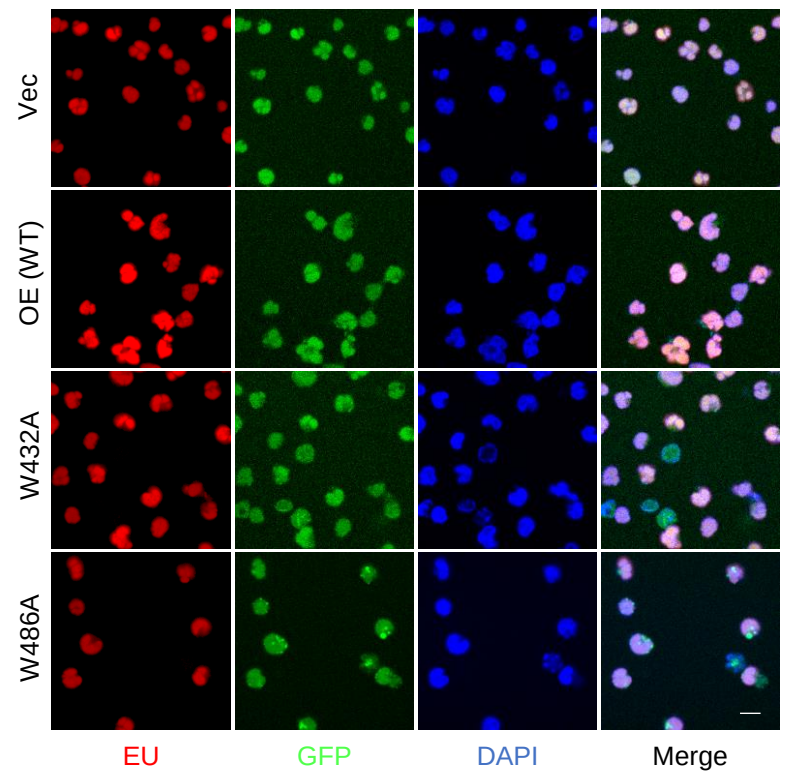
Vec
OE (WT)
W432A
W486A
EU
GFP
DAPI
Merge

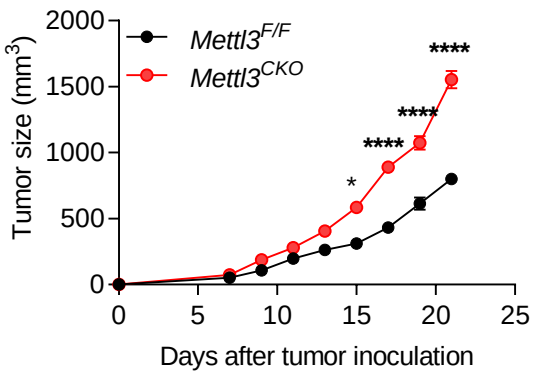
Mettl3F/F
Mettl3CKO
Tumor size (mm3)
Days after tumor inoculation

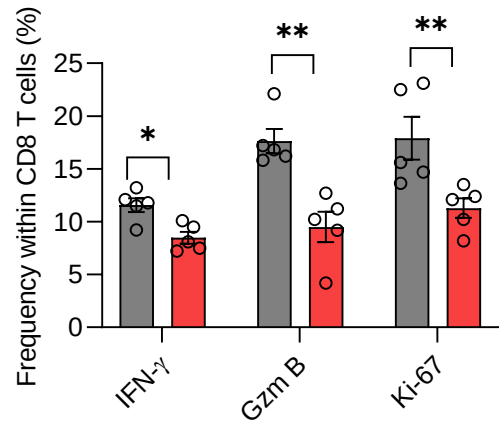
d
Mettl3F/F
Mettl3CKO
Frequency within CD8 T cells (%)
IFN-γ
Gzm B
Ki-67

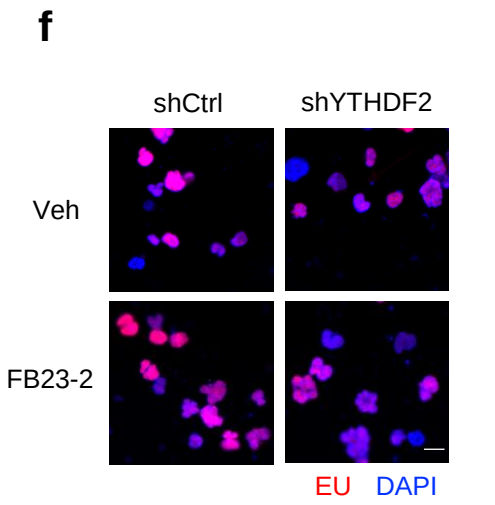
f
shCtrl
shYTHDF2
Veh
FB23-2
EU
DAPI

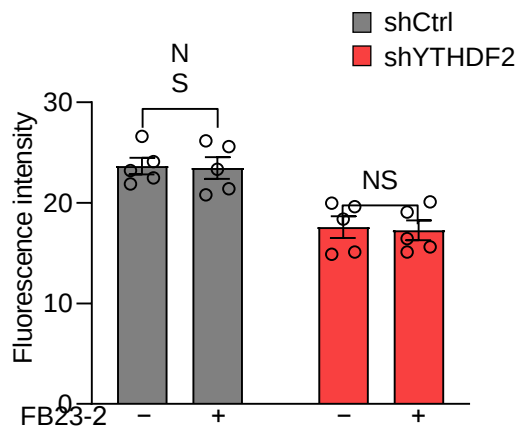
shCtrl
shYTHDF2
N
S
NS
Fluorescence intensity
FB23-2

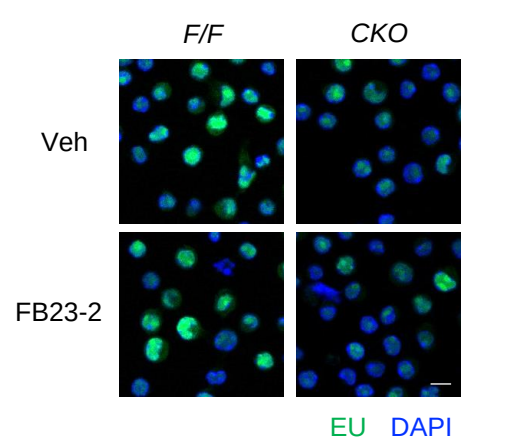
F/F
CKO
Veh
FB23-2
EU
DAPI

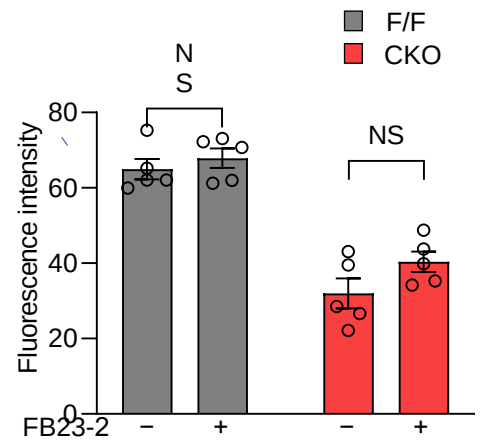
F/F
CKO
N
S
NS
Fluorescence intensity
FB23-2

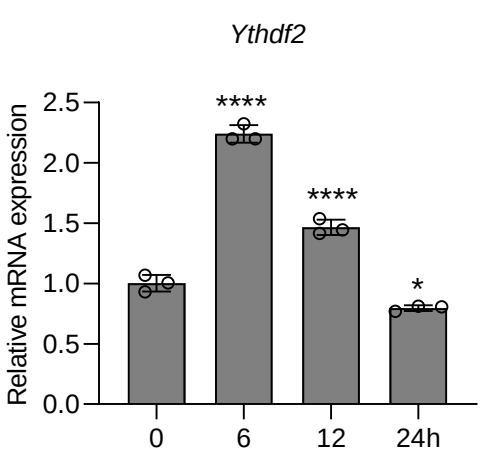
h
Ythdf2
Relative mRNA expression
0
6
12
24h

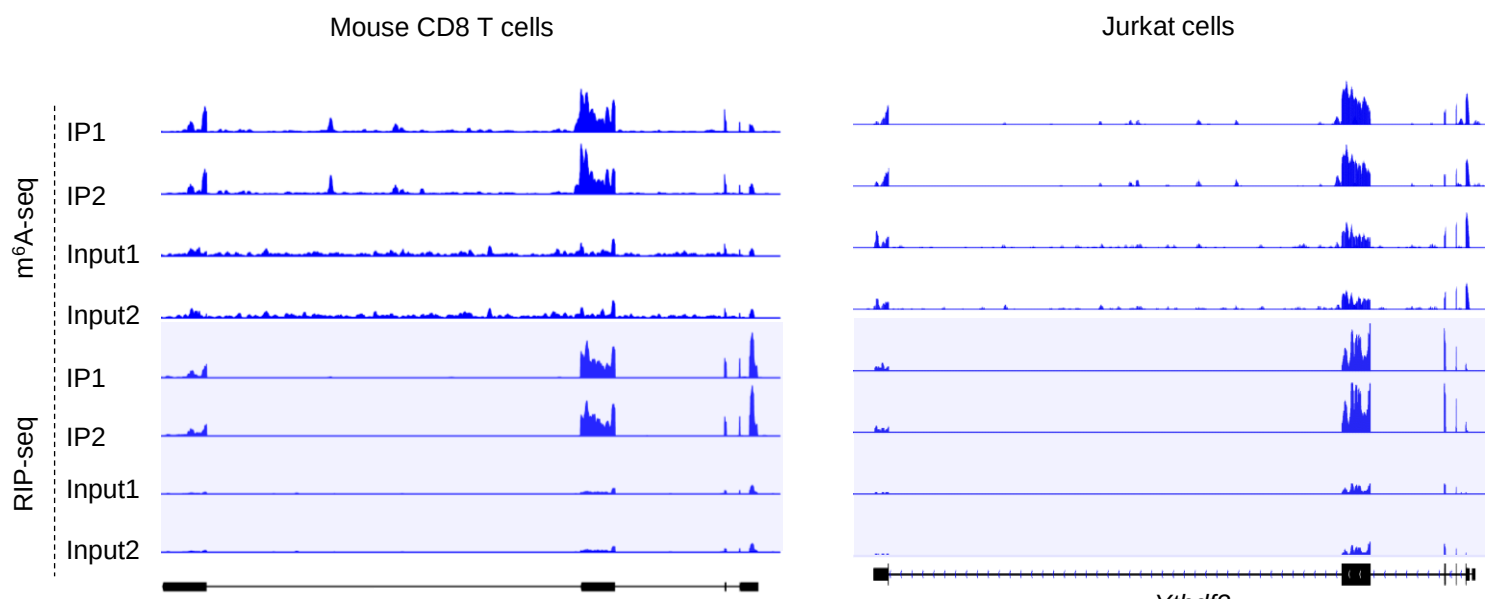
i
Mouse CD8 T cells
Jurkat cells
m6A-seq
RIP-seq
IP1
IP2
Input1
Input2
Ythdf2

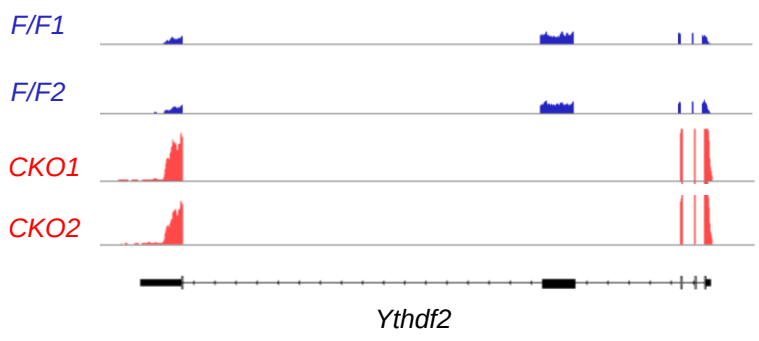
j
F/F1
F/F2
CKO1
CKO2
Ythdf2

Supplementary Fig. 9 | YTHDF2 distribution and expression are governed by the m6A machinery. a Venn diagram showing the overlap of putative YTHDF2-target genes and IKZF1/3-target genes with both enhanced chromatin accessibility and reduced mRNA expression found in *Ythdf2*^{CKO} CD8 T cells. **b** Immunoblotting analysis of METTL3 and GAPDH expression in activated *Mettl3*$^{F/F}$ or *Mettl3*^{CKO} CD8 T cells (anti-CD3/CD28, 5 μg/ml, 24 h). **c** Female *Mettl3*$^{F/F}$ (n = 6) and *Mettl3*^{CKO} (n = 6) mice were injected subcutaneously with 10^6 MC38 cells. Tumor growth was monitored ever 2 or 3 days. **d** TILs were isolated from *Mettl3*$^{F/F}$ (n = 5) and *Mettl3*^{CKO} (n = 5) mice 12 days after MC38 tumor inoculation. Frequencies of CD8 T cell subpopulations positive for Gzm B, IFN-γ, or Ki-67 were assessed by flow cytometry. **e** Click-it RNA imaging and analysis of nascent RNA (red) synthesis in Jurkat cells introduced with WT or mutant YTHDF2. Scale bar, 10 μm (n = 5 per group). **f** Click-it RNA imaging and analysis of nascent RNA synthesis (red) in Jurkat-shCtrl and Jurkat-shYTHDF2 cells in the presence of 10 μM FB23-2 or veh for 72 h (n = 5 per group). Scale bar, 10 μm. **g** Click-it RNA imaging and analysis of nascent RNA synthesis (green) in *Ythdf2*$^{F/F}$ and *Ythdf2*^{CKO} CD8 T cells primed in the presence of 10 μM FB23-2 or veh for 72 h (n = 5 per group). Scale bar, 10 μm. **h** *Ythdf2* mRNA levels detected by qPCR in CD8 T cells stimulated with anti-CD3/CD28 (5 μg/ml) for the indicated amount of time (n = 3 per group). **i** m^{6}A-seq and RIP-seq tracks of *Ythdf2* mRNA loci on mouse CD8 T cells (left) and Jurkat cells (right). **j** RNA-seq tracks of *Ythdf2* mRNA loci on primed*Ythdf2*$^{F/F}$ and *Ythdf2*^{CKO} CD8 T cells. Error bars, mean ± s.e.m. NS, no significance; **P* < 0.05; *****P* < 0.0001. Two-tailed unpaired Student's t-test (d). One-way (e, h) or two-way ANOVA (c, f, g).

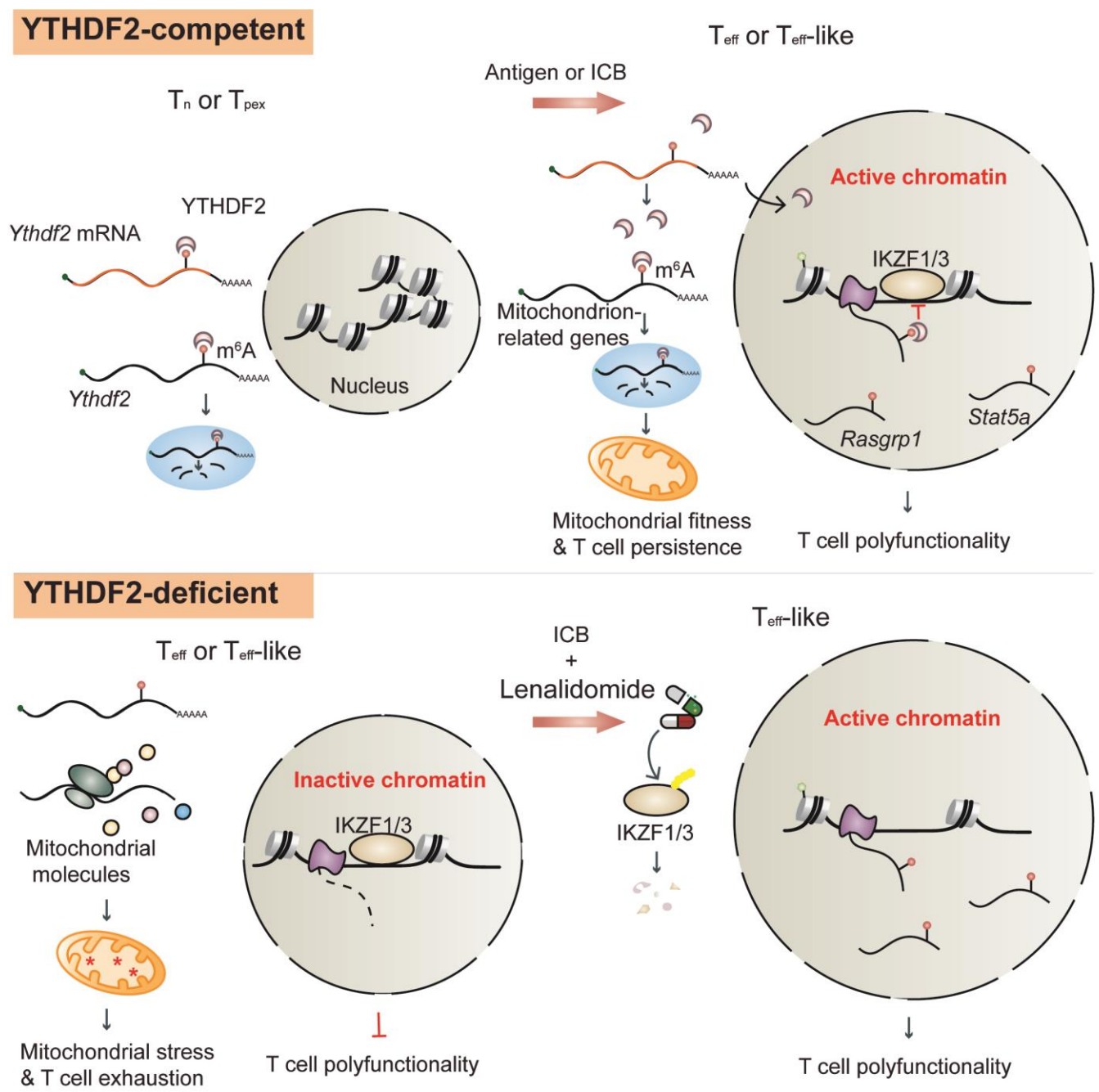

Supplementary Fig. 10 | Schematic diagram of YTHDF2 functioning in antitumor CD8 T cells. Contrary to the autoregulated *Ythdf2* mRNA decay in a quiescent state, YTHDF2 protein is partially relocated and swiftly accumulated upon early CD8 T cell activation or reinvigoration. While cytoplasmic YTHDF2 degrades redundant mitochondrial component-encoding mRNAs to sustain T cell persistence, its nuclear translocation is likely to safeguard T cell effectiveness and ICB responsiveness by minimizing IKZF1/3-mediated transcriptional repression. Conversely, YTHDF2 defect-associated ICB resistance could be overcome by targeting IKZF1/3.

a

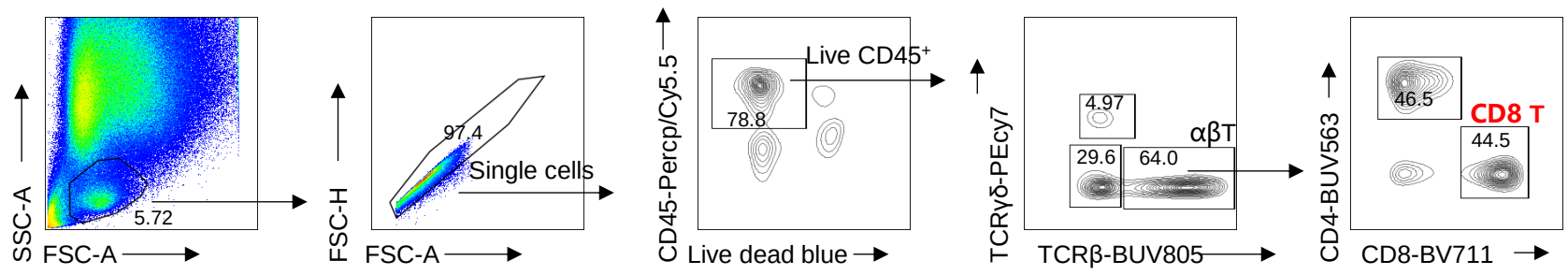

Supplementary Fig. 11 | Flow cytometry gating strategy. a Flow cytometry gating strategy to identify tumor infiltrating CD 8 T cells in this study.